Late Cretaceous gravitational collapse of the southern Sierra Nevada batholith, California

Alan D. Chapman[1,2,*], Jason B. Saleeby[1], David J. Wood[1,†], Alison Piasecki[1], Steven Kidder[1], Mihai N. Ducea[2], and Kenneth A. Farley[1]

[1]*Division of Geological and Planetary Sciences, California Institute of Technology, Pasadena, California 91125, USA*
[2]*Department of Geosciences, University of Arizona, Tucson, Arizona 85721, USA*

ABSTRACT

The Sierra Nevada batholith is an ~600-km-long, NNW-trending composite arc assemblage consisting of a myriad of plutons exhibiting a distinct transverse zonation in structural, petrologic, geochronologic, and isotopic patterns. This zonation is most clearly expressed by a west-to-east variation from mafic to felsic plutonic assemblages. South of 35.5°N, the depth of exposure increases markedly, and fragments of shallow-level eastern Sierra Nevada batholith affinity rocks overlie deeper-level western zone rocks and subjacent subduction accretion assemblages along a major Late Cretaceous detachment system. The magnitude of displacement along this detachment system is assessed here by palinspastic reconstruction of vertical piercing points provided by batholithic and metamorphic pendant structure and stratigraphy. Integration of new and published U-Pb zircon geochronologic, thermobarometric, (U-Th)/He thermochronometric, and geochemical data from plutonic and metamorphic framework assemblages in the southern Sierra Nevada batholith reveal seven potential correlations between dispersed crustal fragments and the Sierra Nevada batholith autochthon. Each correlation suggests at least 50 km of south- to southwest-directed transport and tectonic excision of ~5–10 km of crust along the Late Cretaceous detachment system. The timing and pattern of regional dispersion of crustal fragments in the southern Sierra Nevada batholith is most consistent with Late Cretaceous collapse above the underplated accretionary complex. We infer, from data presented herein (1) a high degree of coupling between the shallow and deep crust during extension, and (2) that the development of modern landscape in southern California was greatly preconditioned by Late Cretaceous tectonics.

*Email: adchapman@email.arizona.edu.
†Present address: 3423 Broadmead Drive, Houston, Texas 77025, USA.

INTRODUCTION

In zones of convergence, regional gradients in gravitational potential energy can be relaxed through lateral spreading and vertical thinning of orogenic crust (e.g., Dewey, 1988; Rey et al., 2001). Deep-crustal exposures of the southern Sierra Nevada batholith, subjacent subduction accretion assemblages, and flanking shallow-level assemblages of the Mojave Desert and Salinian block represent a multi-tiered regional core complex that formed in response to crustal thickening and subsequent extensional collapse (Glazner et al., 1989; Malin et al., 1995; Wood and Saleeby, 1997; Kidder et al., 2003; Saleeby, 2003; Chapman et al., 2010, 2011). The collapse phase is marked by the structural ascent of presently exposed high-pressure (7–11 kbar) rocks of the southern Sierra Nevada batholith and vicinity (Ague and Brimhall, 1988; Pickett and Saleeby, 1993; Fletcher et al., 2002; Grove et al., 2003; Kidder et al., 2003; Saleeby et al., 2007; Nadin and Saleeby, 2008; Chapman et al., 2010, 2011) and the dispersal of lower pressure (2–4 kbar), southeastern Sierra Nevada batholith affinity assemblages across the entire width of the batholith (May 1989; Malin et al., 1995; Wood and Saleeby, 1997; Saleeby, 2003; Chapman et al., 2010).

Dokka and Ross (1995) speculate that extension in the southern Sierra-Salinia core complex is Neogene in age. Glazner et al. (1996) refute this model, arguing that late Cenozoic structures and structural relief in the core complex resulted instead from crustal shortening. We contribute to this debate by showing that major extension and basement rotations in the southern Sierra-Salinia core complex are Late Cretaceous in age. Furthermore, this effort focuses on specific and elusive issues pertaining to Late Cretaceous disruption and dispersion of the southern Sierra Nevada batholith and vicinity, including: (1) the magnitude and timing of tectonic transport of upper crustal fragments along a regional detachment system; (2) the degree of strain coupling between differentially exhuming levels of the crust; (3) the importance of strike-slip faulting during collapse; and (4) the extent to which the development of the southern Sierra Nevada landscape was influenced by Late Cretaceous tectonism.

Major plutonic units and metamorphic pendants of the southern Sierra Nevada batholith are fairly well characterized in terms of geologic, U-Pb zircon, $\delta^{18}O$ zircon, $^{87}Sr/^{86}Sr$ (Sr_i), thermobarometric, paleontologic, and bulk compositional data (Kistler and Peterman, 1973, 1978; Chen and Moore, 1979, 1982; Saleeby et al., 1987, 2007, 2008; Ross, 1989; Kistler and Ross, 1990; Pickett and Saleeby, 1993, 1994; Saleeby and Busby, 1993; Lackey et al., 2005, 2008; Nadin and Saleeby, 2008; Memeti et al., 2010). These data sets reveal a regional primary zonation pattern to the batholith and distinct longitudinal belts of Neoproterozoic to lower Mesozoic metamorphic pendant sequences. In aggregate the pendants and plutons of the southern Sierra Nevada batholith are characterized well enough to recognize allochthonous equivalents.

In this study, we present new: (1) field and structural relations to provide the basis for recognizing potential correlations; (2) U-Pb geochronology of plutonic and detrital zircon populations to identify the age and provenance of displaced plutonic and metamorphic assemblages; (3) thermobarometric work to assess pressure differentials between native and displaced assemblages; (4) major and trace element geochemistry and Sr and Nd isotopic ratios to determine the sources of allochthonous metavolcanic rocks; and (5) zircon (U-Th)/He thermochronometry to constrain the timing of

Geosphere; April 2012; v. 8; no. 2; p. 314–341; doi:10.1130/GES00740.1; 15 figures; 5 tables; 3 plates; 1 supplemental file.

extension. These results are integrated with previous geologic studies and thermobarometric, geochronologic, and geochemical databases in order to recognize allochthon-autochthon pairs and to estimate the magnitude of transport that they imply.

GEOLOGIC BACKGROUND

"Autochthonous" Sierra Nevada Batholith

The Sierra Nevada block is a NNW-trending composite batholith with juvenile batholithic crust extending to ≥35 km depth (Ruppert et al., 1998; Saleeby et al., 2003, 2007). Gradients in pluton ages, integrated bulk compositions, amounts of recycled crustal components, and the paleogeographic affinities of metamorphic pendants define a distinct west to east zonation (Figs. 1 and 2). These zones may be used to recognize and reconstruct superimposed tectonic disruptions.

For convenience, we refer to the pre-Late Cretaceous architecture of the Sierra Nevada batholith and adjacent southern California batholith of the Mojave Desert and Salinia as autochthonous, although a number of the pre-batholithic elements were deformed prior to and during emplacement of the Sierra Nevada batholith (Kistler, 1990; Dunne and Suczek, 1991; Saleeby and Busby, 1993; Stevens and Stone, 2005; Nadin and Saleeby, 2008; Saleeby, 2011; Fig. 2). The following is a summary of key compositional, geochemical, geochronologic, and structural relations between "autochthonous" longitudinal zones of the Sierra Nevada batholith and its framework.

Cretaceous Batholithic Belts

Across-strike variations in composition, pluton emplacement ages, and geochemistry delineate four distinct zones to the Sierra Nevada batholith (Nadin and Saleeby, 2008 and references therein). From west to east, we define the following zones: (1) the ~140–115 Ma dioritic zone, a collection of mafic assemblages dominated by quartz diorite, gabbro, and tonalite, with limited outcrop along the westernmost Sierra Nevada and extensive subcrop beneath the San Joaquin Basin (May and Hewitt, 1948; Williams and Curtis, 1976; Ross, 1989; Saleeby et al., 2009a, 2011); (2) the ~115–100 Ma tonalitic zone with domains of tonalite and lesser amounts of quartz diorite and gabbro; (3) the ~105–90 Ma granodioritic zone rich in mainly tonalite and granodiorite; and (4) ~90–80 Ma granitic zone granodioritic and granitic rocks (Figs. 1 and 3). Initial $^{87}Sr/^{86}Sr$ (Sr_i) increases eastward across the Cretaceous zones from ~0.703 to ~0.709. The boundary between tonalitic and granodioritic zones is generally defined by the Sr_i = 0.706 isopleth (Nadin and Saleeby, 2008).

Pre-Cretaceous Plutons and Metamorphic Framework

Cretaceous plutons of the Sierra Nevada batholith intruded a framework of Neoproterozoic to Mesozoic continental shelf, slope, and rise strata, a belt of accreted abyssal lithosphere, and Triassic to Jurassic plutons, now all exposed as metamorphic pendants (Saleeby et al., 2008; Figs. 1–3). Covariation of pendant stratigraphy, age, and provenance track with plutonic zonation patterns discussed above (Figs. 2 and 3). West to east longitudinal zones include: (1) the Paleozoic Foothills ophiolite belt with overlying Permian to Triassic (?) Calaveras complex hemipelagic deposits, and unconformable infolds of suprasubduction mafic volcanic rocks and siliciclastic turbidites (Saleeby, 2011; Fig. 2). (2) A belt, spanning western to eastern Sierra Nevada batholith zones, of Cambrian to Ordovician eugeoclinal (i.e., deep marine sediments of the outer continental margin) quartzite, phyllite, and chert named the Sierra City mélange and Shoo Fly Complex (e.g., Harding et al., 2000) in the north and the remnants of similar strata preserved in pendants of the Kernville terrane (e.g., Saleeby and Busby, 1993) in the south. (3) Neoproterozoic to Cambrian inner shelf facies of miogeoclinal (i.e., shallow marine sedimentary rocks of the inner continental margin) strata of the Death Valley and Mojave Desert regions, and correlative exposures in the Snow Lake terrane, an allochthonous slice that may have been shuffled ~400 km northward along the cryptic Mesozoic Mojave–Snow Lake fault (Lahren and Schweickert, 1989; Memeti et al., 2010). (4) Neoproterozoic to Cambrian outer shelf miogeoclinal strata of the Inyo facies (Nelson, 1962; Grasse et al., 2001). (5) Cambrian to Devonian eugeoclinal deposits of chert, siliceous argillite, limestone, shale, metaserpentinites, and volcanics belonging to the El Paso terrane (Miller and Sutter, 1982; Carr et al., 1984; Walker, 1988; Martin and Walker, 1995; Gehrels et al., 2000b). The Roberts Mountains allochthon, a similar package of eugeoclinal rocks in Nevada, differs from the El Paso terrane in that the Roberts Mountains allochthon has been thrust over belts (3) and (4) during the Antler orogeny (e.g., Stevens and Greene, 1999; Gehrels et al., 2000a).

Lower Mesozoic sequences of quartzite, carbonate, psammite, pelite, and generally westward-younging Triassic to Cretaceous metavolcanic sequences unconformably overlie Paleozoic strata from western to eastern zones of the Sierra Nevada batholith (Saleeby, 1978, 1987; Walker, 1988; Saleeby and Busby, 1993; Manuszak et al., 2000; Memeti et al., 2010).

Tectonostratigraphy of the Southern Sierra Nevada Region

South of 35.5° N, the depth of exposure increases markedly and the transverse structure of the "autochthonous" Sierra Nevada batholith is disrupted by two major Late Cretaceous systems of parallel low-angle normal faults that juxtapose: (1) subduction accretion assemblages and deep-level exposures of the Sierra Nevada batholith (the Rand fault and Salinas shear zone; Postlethwaite and Jacobson, 1987; Nourse, 1989; Kidder and Ducea, 2006; Chapman et al., 2010, 2011) and (2) eastern and western Sierra Nevada batholith assemblages (the southern Sierra detachment; Wood and Saleeby, 1997; Fig. 1). The resulting generalized tectonostratigraphy of the southern Sierra Nevada batholith, from top to bottom, is that of a multitiered core complex consisting of three packages: allochthonous shallow-level mafic rocks and eastern Sierra Nevada batholith affinity rocks, (par)autochthonous deep-level western Sierra Nevada batholith assemblages, and subduction accretion assemblages. Characteristic features of exposed tectonostratigraphic units and bounding structures in the southern Sierra Nevada batholith and southern California batholith are discussed below.

Mafic Complexes and Cover Strata

The western San Emigdio mafic complex consists of hornblende-hornfels–facies basaltic sheeted dikes and pillows intruded by a suite of mid- to Late Jurassic layered to isotropic gabbroids and lesser amounts of ultramafic cumulates, which in turn are intruded by tonalitic assemblages (Hammond, 1958; James, 1986a; Reitz, 1986; Ross, 1989; Chapman et al., 2010). Correlative rocks of Logan Quarry and Gold Hill continue from the southwesternmost Sierra Nevada batholith into adjacent Salinia (Ross, 1970; Ross et al., 1973; James, 1986a; James et al., 1993).

The contact between the western San Emigdio mafic complex and western Sierra Nevada batholith assemblages is concealed beneath a veneer of Tertiary sedimentary rocks that form the southern margin of the San Joaquin basin. Subcrop mapping indicates that the basement surface is a detachment fault, informally named here as the Maricopa detachment (Fig. 1), consisting of northeast-southwest striated mylonitic and cataclastic assemblages derived from the western Sierra Nevada batholith and the western San Emigdio mafic complex

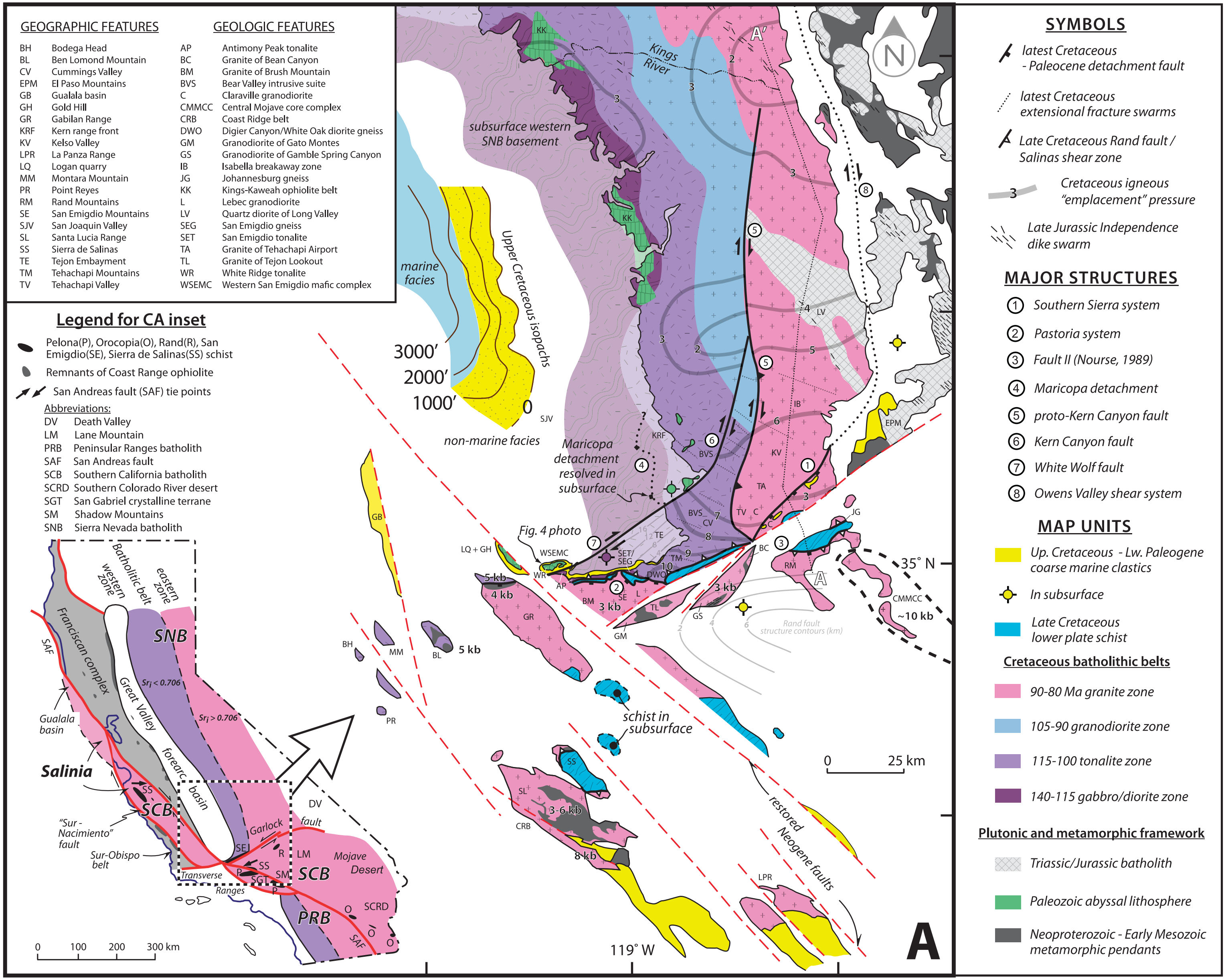

Figure 1 (*on this and following page*). (A) Tectonic map of southern Sierra Nevada basement with related elements of northern Mojave and Salinia restored along San Andreas (310 km of dextral slip removed; Huffman, 1972; Matthews, 1976) and Garlock (50 km of sinistral slip removed; Ross, 1989) faults. Primary zonation and structures of the Sierra Nevada batholith from Saleeby et al. (2007) and Nadin and Saleeby (2008). Pressure determinations from Wiebe (1966, 1970), DeCrisoforo and Cameron (1977), John (1981), Ague and Brimhall (1988), Pickett and Saleeby (1993), Kidder et al. (2003), Nadin and Saleeby (2008), and this study. Extent of the Independence dike swarm from Carl and Glazner (2002), Glazner et al. (2002), Bartley et al. (2007), and Hopson et al. (2008). Rand fault structure contours from Cheadle et al. (1986), Li et al. (1992), Malin et al. (1995), Yan et al. (2005), and Luffi et al. (2009). Subsurface sources from Ross (1989), Monastero et al. (2002), and T. Nilsen (2005, personal commun.). Upper Cretaceous isopachs from Reid (1988).

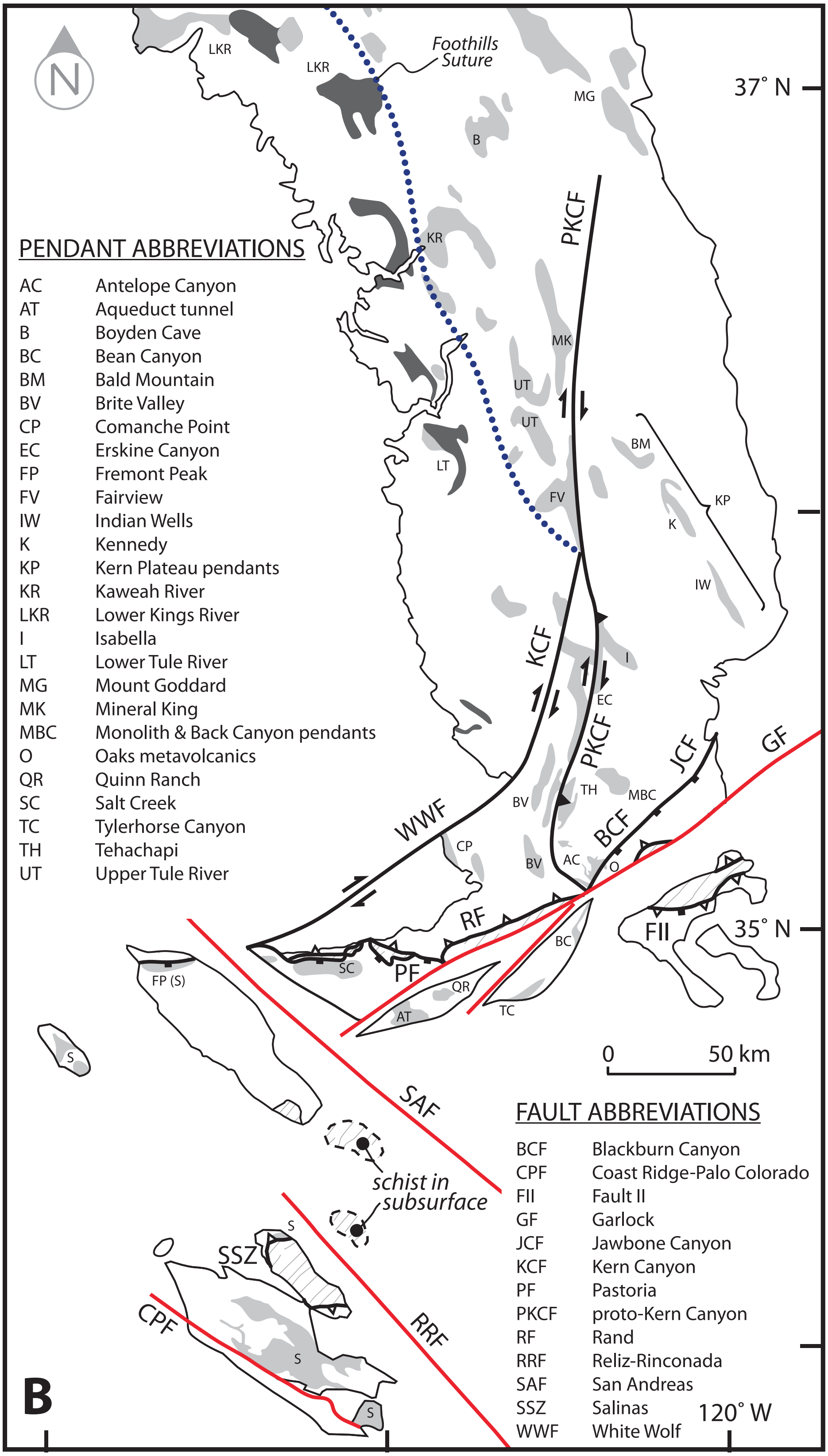

Figure 1 (*continued*). (B) Map showing locations of metamorphic pendants and faults discussed in text. Calaveras complex shown in dark gray; Neoproterozoic to early Mesozoic pendants shown in gray. Cretaceous and Tertiary faults shown in black and red, respectively.

(Saleeby et al., 2009a). The Uvas Member of the Tejon Formation (e.g., Critelli and Nilsen, 2000) unconformably overlies the western San Emigdio mafic complex and contains meter-scale subrounded boulders of western San Emigdio mafic complex material (Fig. 4). The proximity of the Uvas Member to the Maricopa detachment and the presence of large boulders within the unit are consistent with inferred deposition in a supradetachment basin (Wood and Saleeby, 1997).

Eastern Sierra Nevada Batholith–Affinity Shallow-Level Granitoids and Metamorphic Framework Rocks

A first-order feature of the southern Sierra Nevada batholith and vicinity is a tectonostratigraphy topped by crustal fragments of shallow-level granitoids and amphibolite to hornblende hornfels–facies metamorphic pendant rocks (Nourse, 1989; Wood and Saleeby, 1997). These crustal fragments lie in the hanging wall of a regional detachment system consisting of "fault II" of Nourse (1989), the Blackburn Canyon, Jawbone Canyon, and Pastoria faults (Wood and Saleeby, 1997), and the cryptic westward continuation of the Pastoria fault into the Gabilan range (e.g., Kistler and Champion, 2001; Fig. 1A and B). These faults are referred to in aggregate as the southern Sierra detachment system. Here we review key temporal, kinematic, and structural relations of the southern Sierra detachment system.

The southern Sierra detachment system is a complex ductile to brittle low-angle structure that has been differentially remobilized, truncated, and folded by Transverse Ranges contractile deformation. Locally preserved ductile fabrics along eastern elements of the southern Sierra detachment system indicate a top to the south or southeast transport direction (Nourse, 1989; Wood and Saleeby, 1997). Kinematic analysis of the western southern Sierra detachment system is prohibited because original ductile fabrics are severely overprinted in the brittle regime.

Upper and lower plate juxtapositions across the southern Sierra detachment system are profound. These consist of: 2–4 kbar versus 7–11 kbar for pluton emplacement pressures, 87–105 Ma versus 102–138 Ma for pluton emplacement ages, and ~0.708 versus ~0.705 for Sr_i (Saleeby et al., 1987; Kistler and Ross, 1990; Pickett and Saleeby, 1994; Wood and Saleeby, 1997).

Deep-Level Exposures of the Western Sierra Nevada Batholith

Deep-crustal exposures of the Cretaceous batholithic belt lie in the footwall of the southern Sierra detachment system and in the hanging wall of the Rand fault–Salinas shear zone.

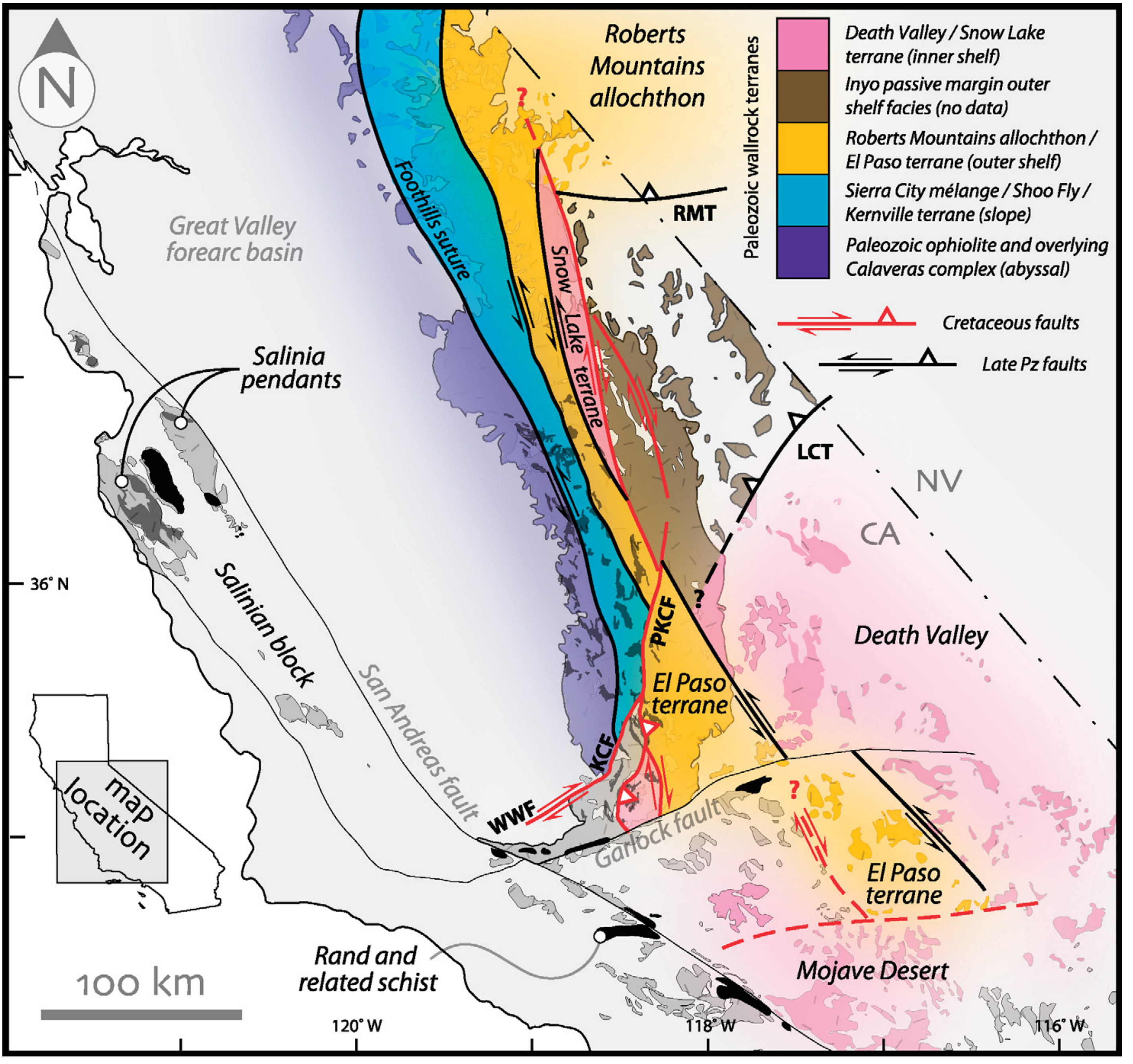

Figure 2. Tectonic map showing paleogeographic affinities of metamorphic pendant belts in the Sierra Nevada batholith. Major Paleozoic and Mesozoic strike-slip faults shown in heavy black and red, respectively. Eugeoclinal assemblages of the El Paso terrane and Roberts Mountains allochthon both shown in orange, despite differences in tectonic setting. Abbreviations: KCF—Kern Canyon fault; LCT—Last Chance thrust; MSLF—Mojave–Snow Lake fault; RMT—Roberts Mountains thrust; WWF—White Wolf fault.

These rocks decrease in thickness and abundance westward from the southern Sierra Nevada batholith into Salinia, where only small remnants are preserved as basement inliers (Kistler and Champion, 2001; Kidder et al., 2003) and conglomerate clasts (Ross et al., 1973; Ross, 1988; James et al. 1993; Schott and Johnson, 1998, 2001; Fig. 1).

Unroofing of deep-level western Sierra Nevada batholith rocks is clearly linked to the transport of upper crustal fragments in the hanging wall of the southern Sierra detachment system. Mated thermochronometric and barometric data for the southern Sierra Nevada batholith, northern Salinia, and the northwestern Mojave Desert show an abrupt Late Cretaceous decompression event coincident with rapid cooling in the deep-level batholithic upper plate (Saleeby et al., 2007; Chapman et al., 2010 and references therein).

Subduction Accretion Assemblages

The Rand, San Emigdio, and Sierra de Salinas schists (referred to in aggregate as "the schist") and similar early Tertiary Pelona and Orocopia

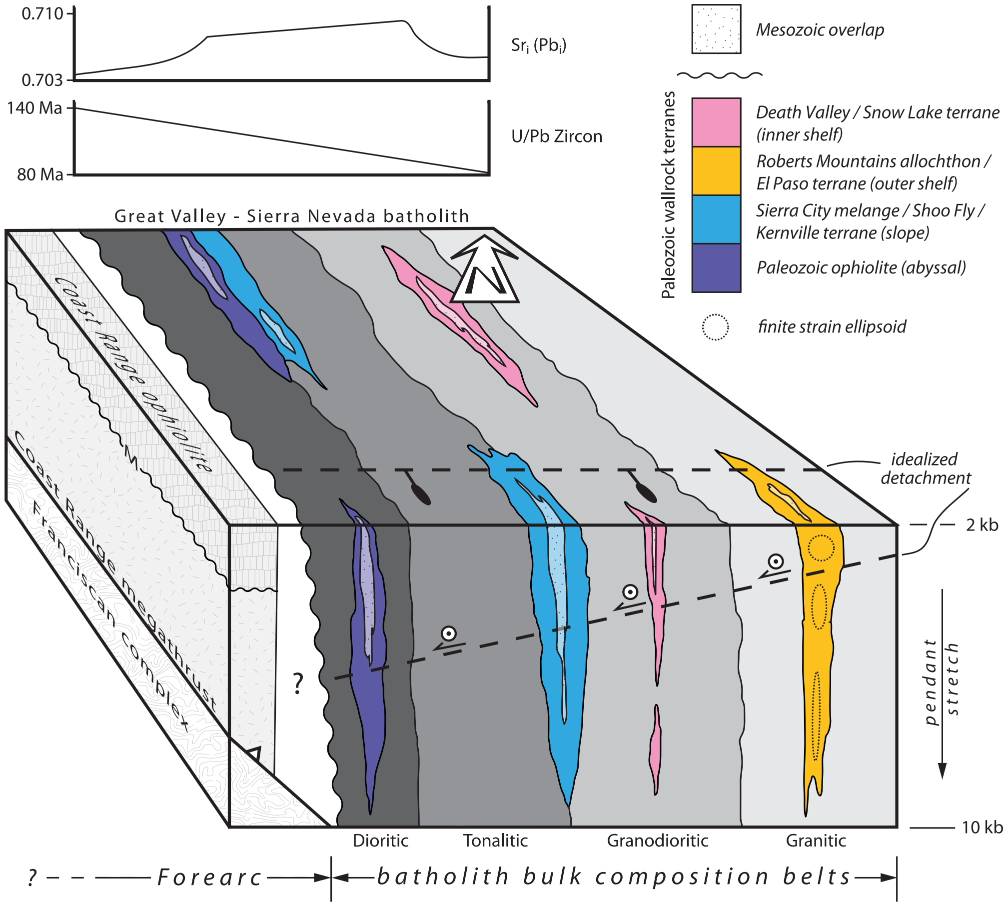

Figure 3. Block diagram illustrating petrologic, isotopic, and age zonation of the Sierra Nevada batholith and the distribution of Paleozoic wall-rock terranes and infolds of lower Mesozoic sedimentary and volcanic protolith sequences immediately prior to Late Cretaceous extensional collapse and activity of the southern Sierra detachment.

schists of more southerly California crop out along detachment structures beneath older crystalline rocks of the southwest Cordilleran batholithic belt (Graham and England, 1976; Haxel and Dillon, 1978; Ehlig, 1981; Jacobson, 1983, 1995; Jacobson et al., 1988, 2007, 2011; Simpson, 1990; Kidder and Ducea, 2006; Ducea et al., 2009; Chapman et al., 2010, 2011). Most workers agree that the deposition and emplacement of the schist occurred during an episode of shallow subduction related to the Laramide orogeny (Jacobson et al., 2007 and references therein).

The deposition, subduction, and structural ascent of the schist are temporally and spatially associated in plate reconstructions with the subduction of a large igneous province (LIP; Saleeby, 2003; Liu et al., 2008, 2010). Subduction of a LIP beneath the southernmost Sierra Nevada batholith and adjacent southern California batholith is hypothesized to have driven slab flattening, leading to the tectonic removal of subbatholithic mantle lithosphere, the cessation of arc magmatism, abrupt crustal thickening in the overriding batholithic plate (Malin et al., 1995; Ducea and Saleeby, 1998; House et al., 2001; Saleeby, 2003; Nadin and Saleeby, 2008) and decompression of batholithic assemblages

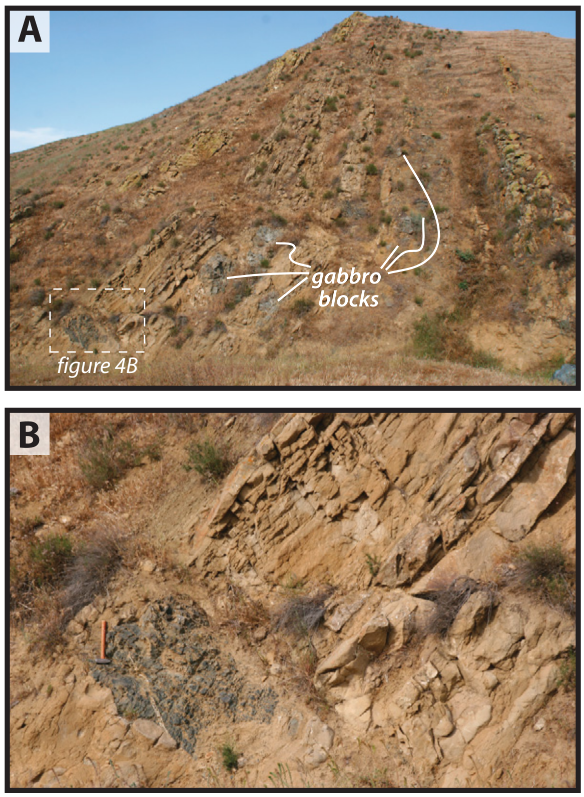

Figure 4. Photographs of Uvas member of the Tejon formation in the San Emigdio Mountains. Note pervasive fracturing of and intrusion of clastic dikes into meter-scale blocks of western San Emigdio mafic complex–derived gabbro. (A) Field of view 50 m long. (B) Field of view 7 m long.

from deep- to midcrustal levels (Saleeby et al., 2007; Chapman et al., 2010). The resultant high-elevation mountain belt segment shed detritus as the schist protolith into the trench, which was immediately underthrust beneath the recently extinguished arc (Kidder and Ducea, 2006).

Late Cretaceous Tectonic Shuffling

Here we review temporal and kinematic relations between the principal members of the integrated proto–Kern Canyon–Kern Canyon–White Wolf fault system (Nadin and Saleeby, 2008) and the Owens Valley shear system (Bartley et al., 2007), because they are important for both the contractile and extensional phases of Late Cretaceous regional deformation in the southern Sierra Nevada batholith. Beginning at ca. 95 Ma, the proto–Kern Canyon fault functioned as a west-directed deep crustal reverse fault with southward increasing throw of 10–25 km and a northward increasing component of dextral shear (Nadin and Saleeby, 2008).

At ca. 88 Ma, the Kern Canyon fault branched from the proto–Kern Canyon fault to the southwest and merged with the proto–White Wolf fault (abbreviated in aggregate as KWF below). Displacement along the KWF increases southward from zero at 36.7° N to 40 km of dextral slip and 15 km of dip slip near the Tejon embayment (Nadin and Saleeby, 2008).

Bartley et al. (2007) show that ~65 km of dextral slip along the Owens Valley shear system occurred between Late Cretaceous and Paleogene time. Coeval shear along the Owens Valley shear system, KWF, and southern Sierra detachment system suggests that these structures may have been cogenetic, with the Owens Valley shear system and KWF representing transfer faults flanking the southern Sierra-Salinia core complex.

RESULTS

Analytical techniques for U-Pb geochronology, (U-Th)/He thermochronometry, thermobarometry, and geochemistry are available in the Supplemental File[1]. Also included in the Supplemental File are complete data sets, sample petrography, representative zircon cathodoluminescence (CL) images and notes, details of the multidimensional scaling algorithm used, a discussion of correlative granitoids, and U-Pb zircon, Sr_i, and igneous and metamorphic pressure databases.

[1]Supplemental File. Zipped file containing supplemental text, Supplemental Figures 1 and 2, Supplemental Movie 1, and Supplemental Tables 1–11. These supplements contain analytical techniques, complete data sets, sample petrography, representative zircon cathodoluminescence (CL) images and notes, details of the multidimensional scaling algorithm used, a movie accompanying Figure 12B, and complete databases accompanying Plates 1, 2, and 3. If you are viewing the PDF of this paper or reading it offline, please visit http://dx.doi.org/10.1130/GES00740.S1 or the full-text article on www.gsapubs.org to view the Supplemental File.

U-Pb Zircon Geochronology

Plutonic Rocks

This geochronologic investigation focuses on batholithic suites adjacent to the southern Sierra detachment system and Maricopa detachment: hanging-wall granitoids of the Pastoria and southern Tehachapi plates, footwall deep-level plutonic assemblages of the San Emigdio Mountains (Tehachapi–San Emigdio complex of Chapman et al., 2010, 2011; Chapman and Saleeby, 2012), and the White Ridge tonalite of the western San Emigdio mafic complex.

Deep-level rocks from the San Emigdio Mountains include: (1) the Antimony Peak tonalite, dated at 131 Ma in reconnaissance U-Pb zircon studies by James (1986a, 1986b); (2) the San Emigdio tonalite, a more felsic phase of the Antimony Peak body; (3) the San Emigdio gneiss (Chapman et al., 2011), an undated hornblende quartz diorite orthogneiss that crops out north of the San Emigdio schist and likely correlates with similar rocks of the 99–105 Ma intrusive suite of Bear Valley (Saleeby et al., 1987; Pickett and Saleeby, 1993; Saleeby et al., 2007); (4) the Digier Canyon diorite gneiss, the western continuation of the White Oak diorite gneiss (Saleeby et al., 2007), a tectonic mixture of amphibolite to locally retrograde greenschist-facies dioritic and subordinate tonalitic, gabbroic, and mylonitic gneisses and cataclasites at the base of the Tehachapi–San Emigdio complex; and (5) the western continuation of the Grapevine Canyon paragneiss (Pickett and Saleeby, 1993, 1994).

Hanging-wall granitoids include: (1) the Lebec granodiorite of Crowell (1952), which hosts the Salt Creek pendant; (2) the Claraville granodiorite of the Blackburn plate, which yields U-Pb zircon ages of 91 ± 1 Ma ~50 km north of our sample site (Saleeby et al., 1987, 2008); (3) the granite of Brush Mountain, assigned a 98 Ma U-Pb zircon age by James (1986b); (4) the granodiorite of Gato Montes, which yields a Rb-Sr isochron age of 96.3 ± 8.7 Ma (Kistler and Ross, 1990); and (5) a hornblende granodiorite in contact with the Tylerhorse Canyon pendant, informally named here the granodiorite of Gamble Spring Canyon. Sample locations and interpreted U-Pb ages of plutonic as well as metavolcanic rocks are given in Table 1 and shown in Plate 1. U-Pb results are shown in Figure 5.

Results from our geochronologic work are combined with all known U-Pb zircon ages from the southern Sierra Nevada and Salinia to produce a color contour map (Plate 1), showing regional variations in pluton emplacement age, using the spatial analyst extension of Arcmap 9 and employing "barriers" such as the proto–Kern Canyon fault, KWF, and other faults shown on Figure 1. Sr_i (Plate 2) and pluton emplacement and metamorphic equilibration pressure (Plate 3) compilation maps were also produced in an identical manner.

Metamorphic Pendant Rocks

A single sample of dacitic metatuff from the Bean Canyon pendant (07TM10) yields a total of 24 concordant analyses with an interpreted age of 273.0 ± 2.4 Ma (Fig. 5). A concordia age of ca. 102.6 ± 1 Ma was determined using two multi-grain zircon fractions from a metamorphosed pumice lapilli silicic tuff (sample 91TH140) from the Oak Creek Pass complex. Thirty-five concordant zircon grains were analyzed from a felsic segregation within the basal amphibolite of the Bean Canyon pendant (11BC1) and give a weighted mean age of 487.4 ± 3.2 Ma.

Samples of metamorphosed siliciclastic rock from the Salt Creek (08SE258), Tylerhorse (08TC44), and Bean Canyon (07BC60) pendants yielded a total of 286 concordant grains suitable for provenance analysis. A normalized probability plot comparing detrital zircon age spectra of samples analyzed here with strata of Death Valley, the Snow Lake terrane, the Salinian block, the Kernville terrane, the El Paso terrane, the Roberts Mountains allochthon, the Sierra City mélange, and the Shoo Fly complex is shown in Figure 6. Sample 08SE258 has major age peaks at ca. 1100 Ma, 1400 Ma, and 1700 Ma. Sample 07BC60 has a major age peak at ca. 1800 Ma, with scattered ages between 1000–1700 Ma and 2300–2900 Ma. Sample 08TC44 contains scattered ages between ca. 200–600 Ma, 1000–1800 Ma, and 2000–2900 Ma.

Figure 7 compares the age spectra of samples from this study with those of a suite of samples from the terranes listed above using multidimensional scaling (MDS). Multidimensional scaling offers an advantage over traditionally used Kolmogorov-Smirnov (K-S) statistical tests in that MDS can be used to produce visual representations of statistical distances between arrays of age data. In other words, MDS calculates a matrix of statistical distances between samples of detrital zircon ages and plots the samples on a map such that the samples that contain similar age spectra are placed close to each other on the map. Multidimensional scaling mapping of data from the El Paso terrane–Roberts Mountains allochthon, Death Valley–Snow Lake terrane,

TABLE 1. SUMMARY OF SAMPLE LOCATIONS, ROCK UNITS, AND U-Pb ZIRCON AGES

Sample	Lithology	Zone	UTM easting	UTM northing	U-Pb zircon age (Ma)
08SE46	Antimony Peak tonalite	11	319551	3864823	Cores: 135.6 ± 2.1 Rims: 103.4 ± 2.3
08SE262	Antimony Peak tonalite	11	308858	3863886	136.4 ± 0.9
08SE451	Antimony Peak tonalite	11	307028	3861038	135.8 ± 1.0
08SE582	Antimony Peak tonalite	11	305678	3860356	134.5 ± 1.0
08SE675	Antimony Peak tonalite	11	324340	3863296	Cores: 136.4 ± 2.1 Rims: 98.5 ± 2.8
07SE94	San Emigdio gneiss	11	314647	3863872	105.8 ± 0.6
08SE450	San Emigdio gneiss	11	307107	3860929	105.1 ± 2.4
08SE674	Digier Canyon and White Oak diorite gneiss	11	324461	3861916	121.3 ± 1.4
08SE679	Digier Canyon and White Oak diorite gneiss	11	325421	3861840	105.2 ± 2.7
04SE5	Lebec granodiorite	11	311257	3858324	91.6 ± 0.7
06SE19a	Lebec granodiorite	11	316199	3864484	91.1 ± 1.7
08SE256	Lebec granodiorite	11	312736	3860408	88.4 ± 1.2
91TH181	Claraville granodiorite	11	371313	3879868	91.91 ± 0.47
93TH417	Claraville granodiorite	11	368657	3878458	91.93 ± 0.56
10TC5	Granodiorite of Gato Montes	11	294640	3863171	92.1 ± 1.0
08TC27a	Granodiorite of Gamble Spring Canyon	11	367862	3870810	146.8 ± 0.4
08SE596	Granite of Brush Mountain	11	297219	3861811	104.5 ± 0.8
09SE23	White Ridge tonalite	11	291420	3867183	155.2 ± 3.4
91TH140	Oaks metavolcanic	11	368664	3881115	102.64 ± 0.97
07TM10	Bean Canyon metavolcanic	11	374359	3872499	273.0 ± 2.4
11BC1	Bean Canyon amphibolite	11	374571	3872044	487.4 ± 3.4

Note: Universal Transverse Mercator (UTM) coordinates are World Geodetic System datum. Isotopic data can be found in Tables SD1 and SD2 in the Supplemental File (see footnote 1).

and northern and southern Sierra produces clusters (Fig. 7) that can be exploited to test provenance hypotheses for unknown samples.

Paleontology

Broken bivalve remains were discovered by undergraduate assistant S. Peek in a hornfelsic calcareous sandstone from the Tylerhorse Canyon pendant (Fig. 8). These remains strongly resemble Early Jurassic bivalves of the genus Weyla that were recovered from two locations in the same stratigraphic horizon of the Isabella pendant (Saleeby and Busby, 1993; identified by J.W. Durham and D.L. Jones). In each pendant, bivalve fragments are located in a centimeter- to meter-scale layered quartzite unit characterized by thin, calc-silicate and psammitic interbeds that sit stratigraphically above a thick highly recrystallized gray marble. The Isabella pendant fossils are from ~10 and ~50 m above the marble, and the Tylerhorse Canyon fossils are from ~40 m above the marble. These relations suggest stratigraphic equivalence of marble-layered quartzite units in Isabella and Tylershorse Canyon pendants.

(U-Th)/He Thermochronometry

(U-Th)/He zircon ages were determined along a traverse across the footwall of the southern Sierra detachment system from a subset of samples studied by apatite He (see Mahéo et al., 2009 for details and sample locations). Equal elevation and vertical transect sampling traverses are included in the data (Table 2).

Figure 9A shows apatite He ages plotted against sample elevation and zircon He ages adjusted to a "pseudo-elevation" calculated by: (1) taking the difference in apatite He and zircon He ages, (2) multiplying this difference by the Cenozoic regional erosion rate (0.05 ± 0.01 mm/yr; Clark et al., 2005; Cecil et al., 2006; Mahéo et al., 2009) to calculate the amount of erosion that took place between apatite He and zircon He closure, and (3) adding the eroded amount to the sample elevation for zircon He determinations. The age-(pseudo)elevation relationships shown in Figure 9A indicate that the footwall of the southern Sierra detachment system cooled through the ~180 °C zircon He closure temperature (Reiners, 2005) rapidly at 77 ± 5 Ma.

K/Ar and Ar/Ar ages on biotite and hornblende scattered across the autochthon are in the 89 to 75 Ma range (Kistler and Peterman, 1978; Dixon, 1995). These ages, when coupled with zircon U-Pb igneous and He cooling ages, further indicate cooling from solidus conditions to He zircon closure at ~100 °C/m.y. scale (Fig. 9B).

Thermobarometry

The rationale behind our thermobarometric work is that correlative native and displaced sites should show pressure differentials that reflect the relative upper and lower plate positions. To investigate igneous emplacement pressures as well as peak metamorphic conditions within pendant rocks, a suite of samples was collected from the southern Tehachapi Mountains, San Emigdio Mountains, and the Santa Lucia Range. Pressure-temperature conditions for metapelitic pendant rock were calculated from garnet + biotite + plagioclase + quartz ± sillimanite/andalusite ± cordierite ± K-feldspar (Table 3) assemblages interpreted to have equilibrated during peak metamorphism. Calculated temperatures and pressures for metapelitic pendant rock range from ~550 to 700 °C and 2.5 to 4 kbar.

Host plutons containing the equilibrium assemblage hornblende + plagioclase + K-feldspar + quartz + sphene + iron titanium oxide were collected for aluminum-in-hornblende (Al-in-hbl) igneous barometry (Hammarstrom and Zen, 1986; Hollister et al., 1987; Johnson and Rutherford, 1989; Schmidt, 1992; Anderson and Smith, 1995; Ague, 1997). We report hornblende-plagioclase temperatures as well as Al-in-hbl pressures for Hammarstrom and Zen (1986), Hollister et al. (1987), Johnson and Rutherford (1989), Schmidt (1992), and Anderson and Smith (1995) calibrations in Table 4. Thermobarometric results are appended to a recent compilation by Nadin and Saleeby (2008) to produce a color contour map (Plate 3), showing regional variations in igneous and metamorphic pressure for the southern Sierra Nevada batholith and Salinia. We refer below to the Schmidt (1992) determinations to remain consistent with the Nadin and Saleeby (2008) compilation.

Geochemistry

Western San Emigdio Mafic Complex

Major and trace element geochemistry and Sr and Nd isotopic ratios were determined from allochthonous metavolcanic rocks to evaluate the most likely native sites of these rocks. Major and trace element data indicate that sheeted dikes and pillow basalts from the western San Emigdio mafic complex are of normal mid-ocean ridge basalt (N-MORB) affinity (Sun and McDonough, 1989), with SiO_2 of

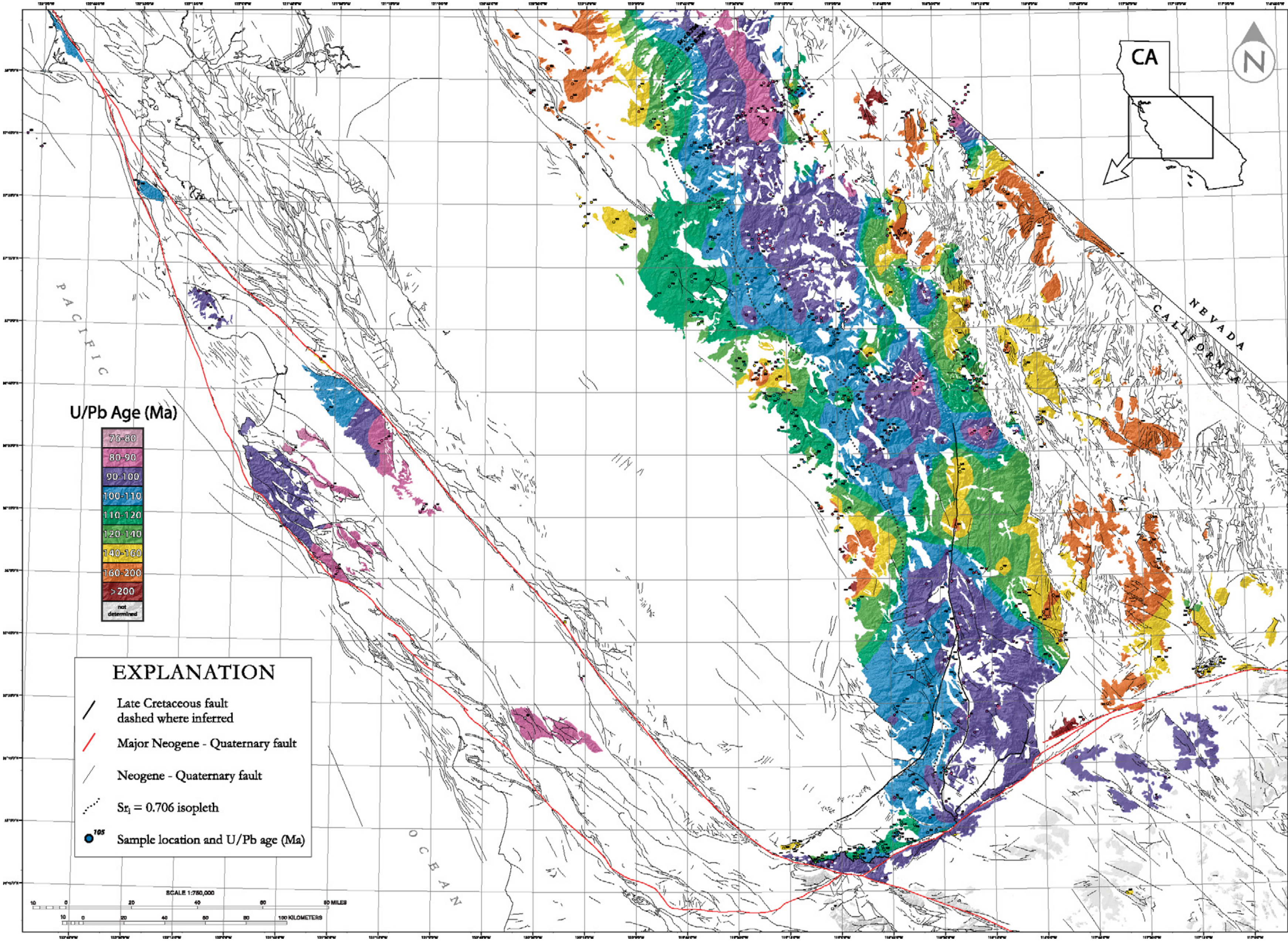

Plate 1. Color contour map showing regional variations in compiled U-Pb zircon ages from plutonic rocks of the Sierra Nevada batholith, Salinian block, and Mojave Desert draped over a digital elevation model. Data, sample locations, and references in Table SD4 in the Supplemental File (see footnote 1). If you are viewing the PDF of this paper or reading it offline, please visit http://dx.doi.org/10.1130/GES00740.S2 or the full-text article on www.gsapubs.org to view Plate 1.

~49 wt%. Trace element data for these rocks are normalized to N-MORB on Figure 10A and shown with the compositional trend of enriched MORB (E-MORB) as well as the range of data from the Paleozoic Kings-Kaweah ophiolite of the Foothills belt (Saleeby, 2011) abundances underlain for comparison. Compositional trends of western San Emigdio mafic complex basalts lie between N-MORB and E-MORB with positive compositional spikes in Cs, Ba, U, K, Pb, and Sr.

The relationship between $^{143}Nd/^{144}Nd$ and $^{87}Sr/^{86}Sr$ supports a MORB origin for the western San Emigdio mafic complex basalts. Initial εNd and $^{87}Sr/^{86}Sr$ (Sr_i) values, age corrected for 160 Ma (the intrusion age of tonalite and gabbro of the western San Emigdio mafic complex) and 484 Ma (the age of basalt-gabbro blocks of the Kings-Kaweah ophiolite belt), range from: εNd_{160} = +9.3 to +13.7, εNd_{484} = +11.3 to +15.9, $^{87}Sr/^{86}Sr_{160}$ = 0.7033 to 0.7035, and $^{87}Sr/^{86}Sr_{484}$ = 0.7032 to 0.7033 (Supplemental Table 11 in the Supplemental File [see footnote 1]), indicating that western San Emigdio mafic complex basalts were derived from a source with long-term large ion lithophile element depletion, like that of convecting mantle beneath the Pacific Ocean basin (Hofmann, 2003). This is consistent with the trace element patterns of Figure 10A, and with primitive mantle normalized La/Sm values of 0.67–0.72 at high initial εNd, which also plot within the field of modern Pacific MORB (Hofmann, 2003) and reflect long-term large-ion lithophile element depletion of the mantle source.

Bean Canyon Metavolcanic Rocks

Approximately 150 m of silicic metavolcanic rock crop out near the top of the Bean Canyon pendant section. Geochemical analysis of Bean Canyon metavolcanic rocks indicates that they are medium- to high-K dacite with ~66 wt% SiO_2. Figure 10B is an N-MORB–normalized spidergram comparing the trace element patterns of Bean Canyon pendant metatuffs and dacitic to rhyolitic metatuffs of the Kennedy pendant (Dunne and Suczek, 1991). Compositional trends of metatuff suites overlap, with prominent troughs in Nb, P, and Ti and a peak in K. An additional peak in Pb is detected in Bean Canyon metavolcanic rocks. Subduction-related volcanic rocks commonly exhibit similar Nb and Pb spikes, as well as spikes in mobile elements such as K (e.g., Hofmann, 2003). AFM and Ti versus Zr diagrams (Pearce et al., 1981) support the view that Bean Canyon and Kennedy pendant metavolcanic rocks resulted from suprasubduction zone magmatism, with data plotting within calc-alkaline (Fig. 11A) and arc volcanic (Fig. 11B) fields.

DISCUSSION

Palinspastic Restoration of Vertical Piercing Points

Integrated field mapping, petrography, geochronology, and geochemistry reveal seven distinctive allochthonous assemblages that may correlate with similar autochthonous rocks of the southern Sierra Nevada and vicinity. Wood and Saleeby (1997) argued on the basis of geologic evidence for an additional nine correlations, two of which are supported by this study (correlations 2 and 3, described below) and two are modified slightly (correlations 1 and 5). All correlations are summarized in Table 5 and shown on Figure 12A.

Correlation #1: Area between Lake Isabella and Kern Plateau Pendants (A) and Bean Canyon and Tylerhorse Canyon Pendants (A′)

The Bean Canyon pendant is characterized by a succession of marble, quartzite, calc-silicate hornfels, pelitic schist, and silicic metatuff, unconformably underlain by amphibolite and associated ultramafic rock (Rindosh, 1977; Ross, 1989; Wood and Saleeby, 1997; and this study). We report an Early Ordovician (487.4 ± 3.4 Ma) U-Pb zircon age from the basal amphibolite unit. An overlapping Sm-Nd isochron age of 484 ± 18 Ma from the Kings River ophiolite (Saleeby, 2011) suggests a possible relationship, currently under investigation, between mafic rocks at the base of the Bean Canyon section and the Kings River ophiolite. The correlation of metamorphosed mafic to ultramafic bodies in Bean Canyon and Salinia with similar rocks at the apparent base of the Kennedy pendant section in the El Paso terrane is discussed below in "correlation #5."

Detrital zircon geochronologic data reported herein indicate that quartzite (sample 07BC60) from the Bean Canyon pendant contains an age distribution similar to that of eugeoclinal deposits of the El Paso terrane (J. Saleeby, 2011, personal commun.) and Roberts Mountains allochthon (Gehrels et al., 2000a) and miogeoclinal rocks of the Snow Lake pendant (Figs. 6 and 7). A U-Pb zircon age of 273.0 ± 2.4 Ma for dacitic metatuff from near the top of the Bean Canyon section overlaps in age with andesitic flows and breccias from the El Paso Mountains (Walker, 1988; Martin and Walker, 1995) and indicates that the Bean Canyon pendant is entirely Paleozoic. Trace element abundances of undated silicic metavolcanic rocks from the Kern Plateau resemble those of the Bean Canyon pendant (Fig. 10B). Age, geochemical, petrographic, and stratigraphic relations lead us to suggest that volcanic and metavolcanic rocks exposed in the El Paso Mountains, and Bean and Kern Plateau pendants are correlative.

The Tylerhorse Canyon pendant lies stratigraphically above the Bean Canyon pendant and consists of pelitic and psammitic schist, calc-silicates, and marble. The U-Pb detrital zircon age spectrum from metapsammitic sample 08TC44 partially overlaps that of sample 07BC60 from the Bean Canyon pendant for grains older than ca. 1400 Ma (Fig. 6), but abundant late Paleozoic to early Mesozoic grains indicate that strata of the Tylerhorse Canyon pendant were deposited into Jurassic time. The Tylerhorse Canyon section is, therefore, interpreted as a Mesozoic overlap sequence deposited across Bean Canyon pendant protoliths.

A similar depositional setting is envisaged for the Isabella pendant, based on the presence of Paleozoic amphibolite overlain by Triassic to Jurassic metavolcanic and metasedimentary rocks. Fossils that resemble the Early Jurassic pectinid bivalve Weyla (Fig. 8) corroborate a Mesozoic depositional age for Tylerhorse Canyon strata and permit correlation to equivalent strata found in the Lake Isabella pendant.

Two igneous suites of distinct age and composition intrude the Bean Canyon–Tylerhorse Canyon package. First is a series of east-striking tonalitic, gabbroic, and granodioritic dikes and lenticular masses distributed throughout and along the margins of the pendants. The granodiorite of Gamble Spring Canyon represents one phase of the suite, and with a U-Pb zircon emplacement age of 146.8 ± 0.4 Ma, is similar in age to the quartz diorite of Long Valley (J. Saleeby, 2011, personal commun.) and to the

Figure 5 (*on following two pages*). (A) U-Pb age-frequency spectra (after Ludwig, 2003) from laser ablation–inductively coupled plasma–mass spectrometry data on 18 samples from the Sierra Nevada batholith. Errors are 2σ. Abbreviations for rejected grains: HE—high $^{206}Pb/^{238}U$ error; I/E—source inheritance and/or entrainment; IN—inclusion(s) overlapped during ablation; LL—lead loss; OL—analysis of overlapping age domains. (B) Tera-Wasserburg diagrams and concordia intercept ages (after Ludwig, 2003) from isotope dilution–thermal ionization–mass spectrometry data on three samples from the southern Sierra Nevada batholith. Errors are 2σ. Isotopic data in Tables SD1 and SD2 in the Supplemental File (see footnote 1). MSWD—Mean square of weighted deviates.

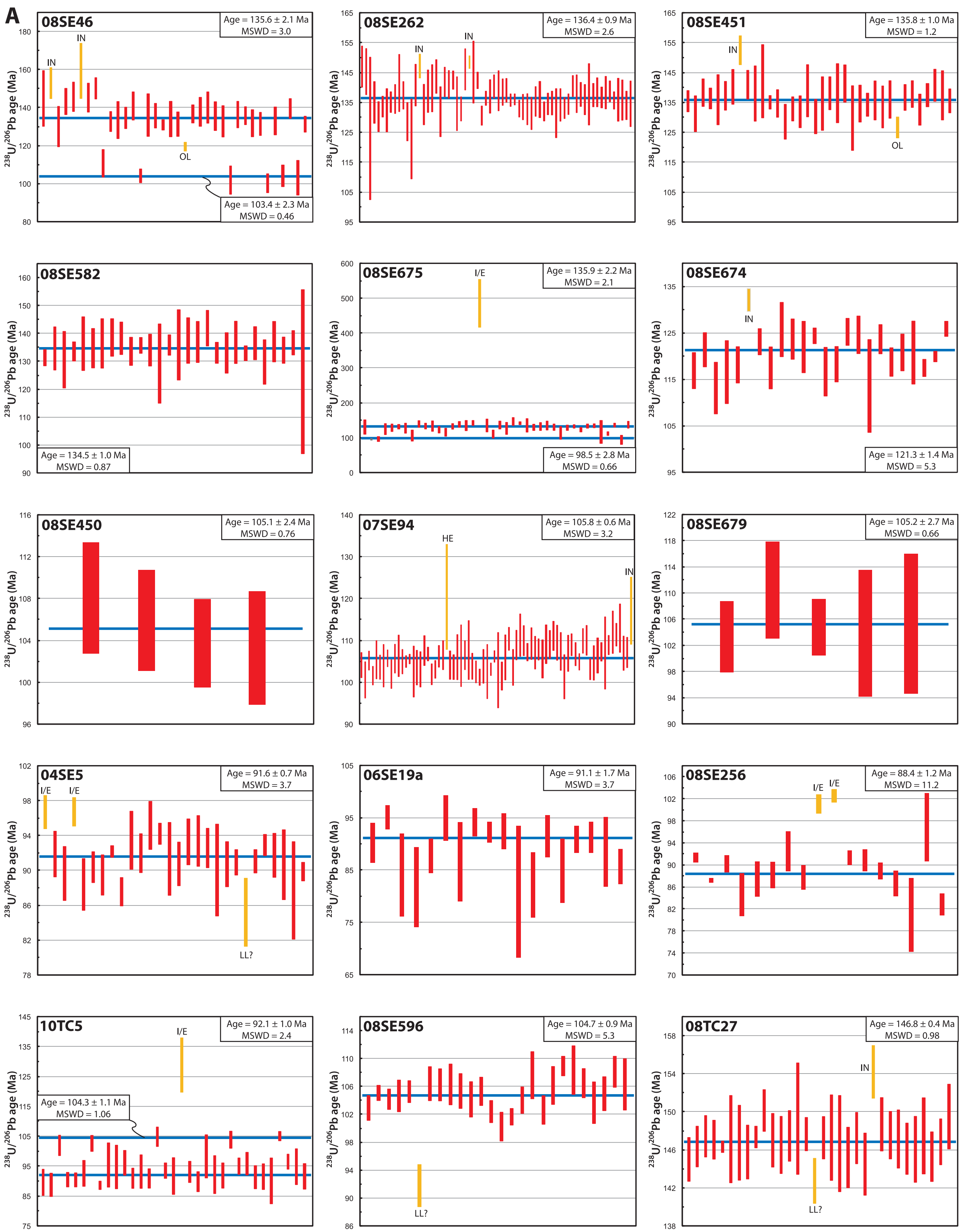
A
08SE46
Age = 135.6 ± 2.1 Ma
MSWD = 3.0
Age = 103.4 ± 2.3 Ma
MSWD = 0.46
IN
OL
08SE262
Age = 136.4 ± 0.9 Ma
MSWD = 2.6
IN
08SE451
Age = 135.8 ± 1.0 Ma
MSWD = 1.2
IN
OL
08SE582
Age = 134.5 ± 1.0 Ma
MSWD = 0.87
08SE675
Age = 135.9 ± 2.2 Ma
MSWD = 2.1
Age = 98.5 ± 2.8 Ma
MSWD = 0.66
I/E
08SE674
Age = 121.3 ± 1.4 Ma
MSWD = 5.3
IN
08SE450
Age = 105.1 ± 2.4 Ma
MSWD = 0.76
07SE94
Age = 105.8 ± 0.6 Ma
MSWD = 3.2
HE
IN
08SE679
Age = 105.2 ± 2.7 Ma
MSWD = 0.66
04SE5
Age = 91.6 ± 0.7 Ma
MSWD = 3.7
I/E
LL?
06SE19a
Age = 91.1 ± 1.7 Ma
MSWD = 3.7
08SE256
Age = 88.4 ± 1.2 Ma
MSWD = 11.2
I/E
10TC5
Age = 92.1 ± 1.0 Ma
MSWD = 2.4
Age = 104.3 ± 1.1 Ma
MSWD = 1.06
I/E
08SE596
Age = 104.7 ± 0.9 Ma
MSWD = 5.3
LL?
08TC27
Age = 146.8 ± 0.4 Ma
MSWD = 0.98
IN
LL?
$^{238}U/^{206}Pb$ age (Ma)

Figure 5.

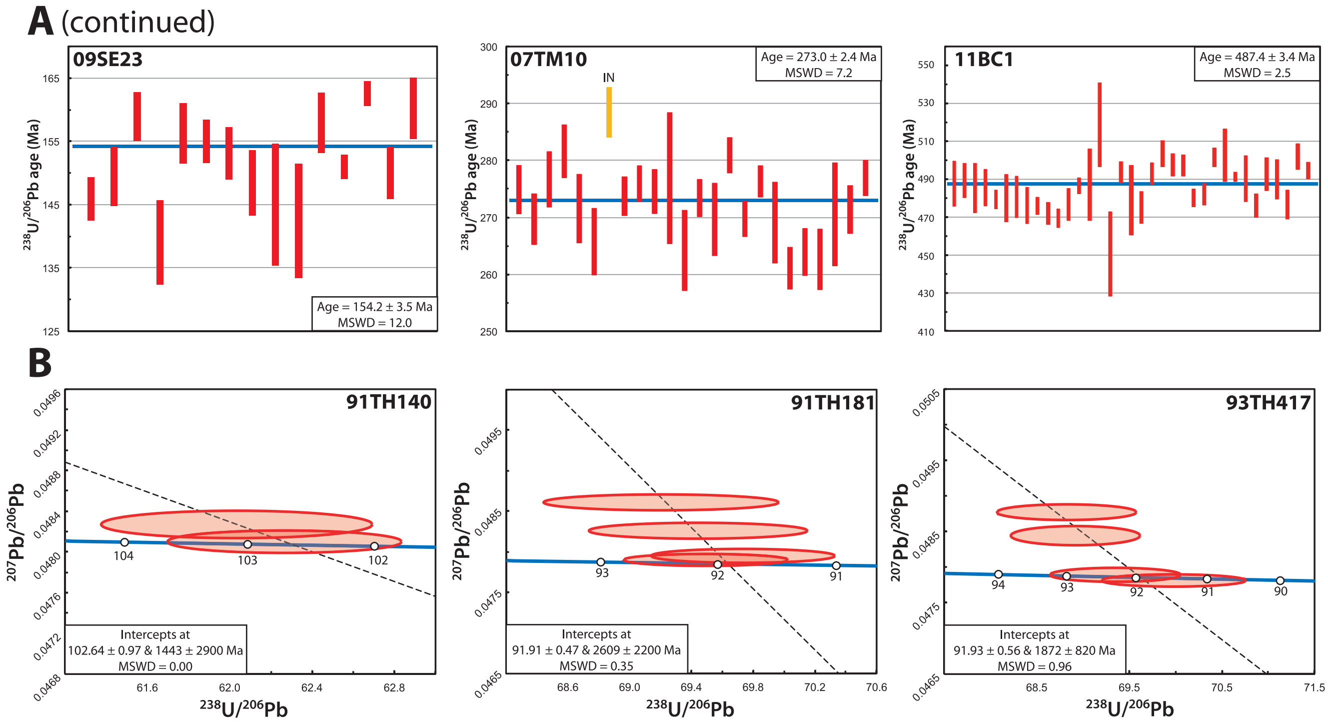

Figure 5 (*continued*).

Late Jurassic Independence dike swarm of the eastern Sierra Nevada–Owens Valley–Mojave Desert region (Chen and Moore, 1979; Carl and Glazner, 2002; Glazner et al., 2002; Bartley et al., 2007; Hopson et al., 2008; Fig. 1). The granodiorite of Gato Montes and granite of Bean Canyon, both Late Cretaceous in age (Evernden and Kistler, 1970; Kistler and Ross, 1990, and this study), comprise a second plutonic suite that intrudes Bean Canyon and Tylerhorse Canyon pendants and the Jurassic granodiorite of Gamble Spring Canyon. High Sr_i ratios (>0.707) characterize these plutons and autochthonous equivalents. An upper plate (a′)–lower plate (a) pressure differential of ~2.4–2.8 kbar (samples 08TC27a and 08TC29; Tables 3 and 4) versus 4.1–5.5 kbar (Nadin and Saleeby, 2008, samples 03SS1, 04SS31, and 51) suggests the removal of 5–10 km of crust along the southern Sierra detachment system during faulting.

Correlation #2: Silicic Metavolcanic Rocks of the Erskine Canyon Sequence (B) and the Oak Creek Pass Complex (B′)

Small screens of finely recrystallized laminated tuffs with remnants of quartz phenocrysts and pumice lapilli crop out in the Oak Creek Pass complex (Wood, 1997; Wood and Saleeby, 1997). The Oaks metatuffs are similar in petrography, texture, and field setting to the 102–105 Ma Erskine Canyon rhyolitic to andesitic metavolcanic sequence, which has been transposed along the proto–Kern Canyon fault over ~40 km adjacent to Lake Isabella (Nadin and Saleeby, 2008; Saleeby et al., 2008). We hypothesize that Oaks metavolcanic rocks represent Erskine Canyon rocks formerly situated east of the proto–Kern Canyon fault that were displaced southward by detachment faulting. U-Pb zircon geochronology reported here supports this view, with an interpreted eruption age of 102.6 ± 1.0 Ma for Oaks metavolcanic rocks.

Pressure determinations from plutons and metamorphic assemblages in contact with Erskine Canyon metavolcanic rocks range from 6.6 to 4.5 kbar (Nadin and Saleeby, 2008, Plate 3), in contrast to 3 to 4.4 kbar determinations from the Claraville granodiorite in the hanging wall (Nadin and Saleeby, 2008, sample RB020601, and samples 93TH417 and 91TH181; Table 4), which intrudes Oaks metavolcanic rocks, corresponding to ~0–12 km of missing crust.

Correlation #3: Monolith and Back Canyon Pendants (C) and Quinn Ranch and Aqueduct Tunnel Pendants (C′)

The Quinn Ranch and Aqueduct Tunnel pendants are characterized by sequences of chiefly marble interleaved with calc-silicate and minor quartzite and siliceous meta-argillite (Ross, 1989). The granodiorite of Gato Montes intrudes these pendants and yields a U-Pb zircon age of 92.1 ± 1.0 Ma. The Aqueduct Tunnel and Quinn Ranch pendants, neighboring small marble septa, and host plutons share similar pendant-pluton relations with Monolith and Back Canyon pendants and intrusive Claraville granodiorite of the south-central Sierra Nevada batholith. A similar range of lithologies to that of Aqueduct Tunnel and Quinn Ranch pendants is seen in Monolith and Back Canyon pendants (Wood and Saleeby, 1997). We suggest, on the basis of distinctive marble successions found in pendants at c and c′, that these pendants belong to the Death Valley facies of the passive margin as exposed in the Shadow Mountains of the western Mojave Desert (Martin and Walker, 1995; Fig. 1). Al-in-hbl pressures of 5.7–6.5 kbar are calculated from the Claraville granodiorite near Kelso Valley in the footwall of the southern Sierra detachment system (Ague and Brimhall, 1988, sample 420; Dixon, 1995, samples 49 and Th275; Nadin and Saleeby, 2008, sample 04SS34). The presence of prograde andalusite as the only stable aluminosilicate phase in pelitic assemblages near c′ (Ross, 1989) suggests that these rocks were intruded and contact metamorphosed at pressures no greater than ~4 kbar (Spear, 1993). These relations suggest the excision of at least 5.5 km of crust along the southern Sierra detachment system.

Correlation #4: Antelope Canyon Group (D) and Salt Creek Pendant (D′)

The Salt Creek pendant of the San Emigdio Mountains is composed principally of layers

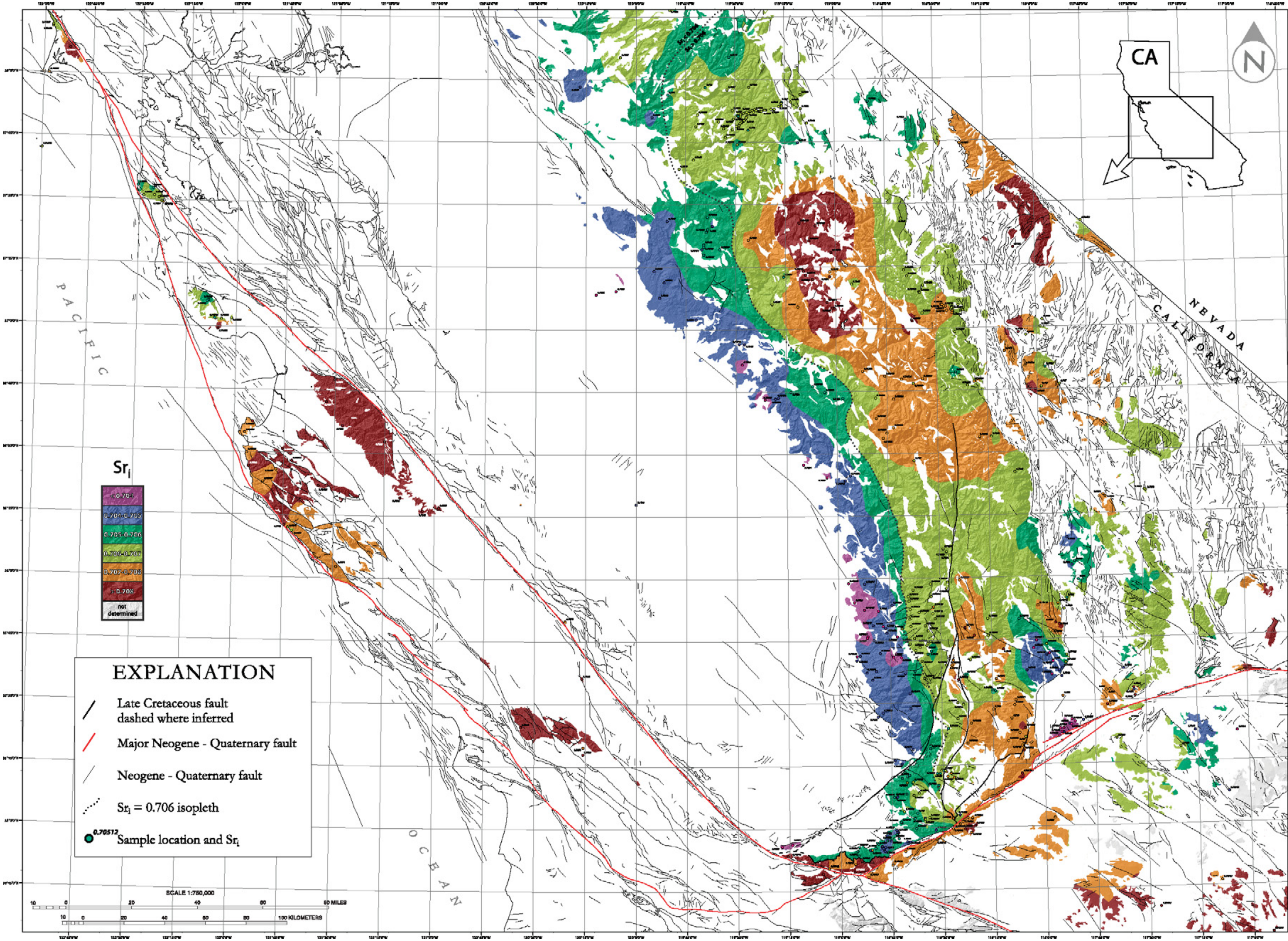

Plate 2. Color contour map showing regional variations in compiled Sr_i ratios from plutonic rocks of the Sierra Nevada batholith, Salinian block, and Mojave Desert draped over a digital elevation model. Data, sample locations, and references in Table SD5 in the Supplemental File (see footnote 1). If you are viewing the PDF of this paper or reading it offline, please visit http://dx.doi.org/10.1130/GES00740.S3 or the full-text article on www.gsapubs.org to view Plate 2.

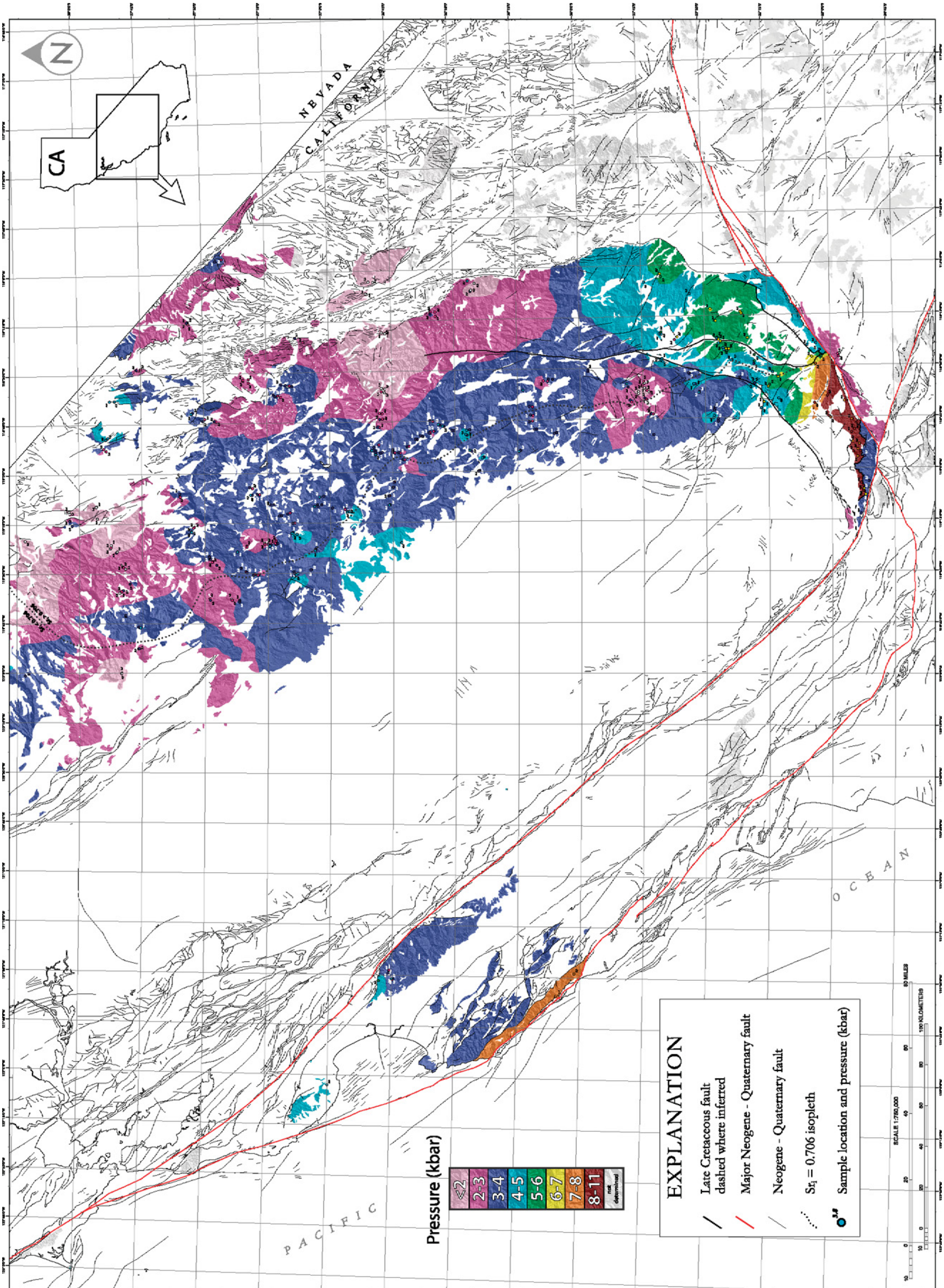

Plate 3. Color contour map showing regional variations in compiled Al-in-hbl emplacement pressures from plutonic rocks and conventional thermobarometric pressure determinations from metamorphic rocks of the Sierra Nevada batholith, Salinian block, and Mojave Desert draped over a digital elevation model. Data, sample locations, and references in Table SD6 in the Supplemental File (see footnote 1). If you are viewing the PDF of this paper or reading it offline, please visit http://dx.doi.org/10.1130/GES00740.S4 or the full-text article on www.gsapubs.org to view Plate 3.

of marble, quartzite, and quartzofeldspathic gneiss, with lesser amounts (<5%) of pelitic to psammitic schist. These lithologies suggest that the protoliths of the Salt Creek pendant were deposited in a slope to inner shelf environment and potentially correlate to similar assemblages found in the Sierra City mélange–Shoo Fly–Kernville terrane (Fig. 2). Our detrital zircon geochronologic data from quartzite sample 08SE258 support this view, with major age peaks corresponding to those of slope strata from the Kernville terrane (Saleeby, 2011; Figs. 6 and 7).

The Salt Creek pendant is intruded by the ca. 90 Ma Lebec granodiorite. Ross (1989) notes lithologic similarities between the Salt Creek pendant and pendants north of Tehachapi Valley, including the Brite Valley, Tehachapi, Monolith, and Back Canyon pendants. However, the Lebec granodiorite-hosted Salt Creek pendant does not likely correlate with Brite Valley and Tehachapi pendants since they are intruded by 99–105 Ma tonalites, diorites, and gabbroids of the intrusive suite of Bear Valley (Saleeby et al., 2007, 2008). In contrast, similar siliciclastic and carbonate rocks of the Antelope Canyon group are intruded by a border phase of the ca. 90 Ma Claraville granodiorite (Wood, 1997), representing the most likely native site for similar assemblages of the Salt Creek pendant and adjacent rocks.

A pressure differential of 6.5 (Dixon, 1995, sample Th275) versus 3.1 (sample 04SE5) and 3.7 (sample 10SE41) kbar (Tables 3 and 4) for autochthonous versus allochthonous assemblages, corresponding to 9–11 km of missing crust, is implied by this correlation.

Correlation #5: Area Southwest of the Rand Mountains (E) and Salinian Framework of the Gabilan Range, Santa Lucia Range, and Southern Ben Lomond Mountain (E′)

The Sur Series (Trask, 1926) of the Santa Lucia and Gabilan Ranges, and smaller exposures in the Ben Lomond and Point Reyes areas, contains abundant interbedded marble and calc-silicate, leading several workers to suggest that metasedimentary rocks of the Salinian block correlate with strata of the Paleozoic Cordilleran miogeocline (e.g., Ross et al., 1973; Ross, 1977; Kidder et al., 2003). However, pure quartzite and marble units that resemble the Stirling and Zabriskie quartzites and the Bonanza King Formation of the Death Valley–Mojave Desert region are conspicuously absent from the Salinian block.

Instead, stratigraphic relations and detrital and igneous zircon ages and pluton geochemistry from northern Salinia and the western Mojave Desert suggest that the El Paso terrane is the most likely parent for "orphan" Salinia. Metasedimentary assemblages of the Salinian terrane share several similarities with eugeoclinal strata of the El Paso terrane. First, thinly-bedded Sur Series assemblages are lithologically similar to strata of the Kern Plateau pendants and the Bean Canyon pendant (Rindosh, 1977; Ross, 1977; Dunne and Suczek, 1991). Second, Sur Series assemblages exhibit broad Late Archean and Proterozoic U-Pb detrital zircon age peaks that roughly correspond to those of the El Paso terrane, including the Bean Canyon pendant (Barbeau et al., 2005; Fig. 6). While Sur Series age peaks are too broad to distinguish between miogeoclinal and eugeoclinal sources within the Mojave Desert, potentially due to zircon isotopic disturbance during high-grade metamorphism, the presence of Permian zircons in Upper Cretaceous cover strata suggests derivation from, or at least proximity to, the El Paso terrane (Barbeau et al., 2005). Lastly, small mafic to ultramafic bodies crop out entirely within, and are elongated parallel to the foliation of, Sur Series metasedimentary rocks (Wiebe, 1966, 1970; Nutt, 1977; Bush, 1981), the Lake Isabella pendant (Saleeby and Busby, 1993), the Bean Canyon pendant (Rindosh, 1977; this study), and the Kern Plateau pendants (Dunne and Suczek, 1991).

The central Santa Lucia and Gabilan Ranges and southern Ben Lomond Mountain contain 93–76 Ma plutons with high Sr_i (typically >0.708; Kistler and Champion, 2001; Kidder et al., 2003; Dickinson et al., 2005) that intruded the Sur Series at pressures of 3.4–4 kbar (John, 1981, and this study). A zone of platformal sequences characterized by quartzite, marble, and psammitic schist (Miller et al., 1995) and high Sr_i and young plutons (Plates 1 and 2) southwest of the Rand Mountains appears to be the most likely native site for the central Santa Lucia and Gabilan Ranges. However, Permian metavolcanic rocks and Independence dikes, two striking yet volumetrically minor constituents of the El Paso terrane, are not reported from the Salinian block. These rock types may be absent from the Salinian block or obscured due to poor exposure.

The Coast Ridge Belt, an exposure of orthogneiss and subordinate marble and quartzite (Kidder et al., 2003), probably represents the midcrustal (~7.5 kbar) equivalent of the central Santa Lucia Range. The belt crops out ~5 km to the west of our 3.4 kbar determination and 4–6 kbar estimates of peak metamorphic pressures in the Sur Series by Wiebe (1966, 1970). The pressure gradient between the Coast Ridge Belt and the central Santa Lucia Mountains is explained by Kidder et al. (2003) as the result of regional ~30° to the NE tilt. However, this tilt can only account for an ~3 km (i.e., ~1 kbar) difference over 5 km. Therefore, the pressure difference between the Coast Ridge Belt and the central Santa Lucia Range must have resulted either from structural attenuation or faulting, potentially along the Coast Ridge and/or Palo Colorado faults (Ross, 1976).

We suggest that the Coast Ridge Belt restores to a position along the west flank of the central Mojave metamorphic core complex, possibly correlating with the Johannesburg gneiss in the hanging wall of the Rand fault, with shallow exposures of the central Santa Lucia Range, Gabilan Range, and southern Ben Lomond Mountain lying in fault contact above the belt. Pressure determinations from footwall assemblages southwest of the Rand Mountains are sparse, yet values of ~10 kbar are reported from the central Mojave metamorphic core complex (Henry and Dokka, 1992). A pressure differential of ~2.5 kbar between the Coast Ridge Belt and the central Mojave metamorphic core complex implies the removal of ~8 km of crust along a structure that has not yet been recognized.

Figure 6 (*on following page*). Normalized probability plots comparing zircon ages from this study with spectra from: Paleozoic slope, inner shelf, and outer shelf strata of the Shoo Fly complex and Sierra City mélange (SF + SCM); eugeoclinal strata of the Roberts Mountains allochthon (RMA); Kern Plateau pendants of the El Paso terrane (EP); miogeoclinal strata of Death Valley and the Snow Lake terrane (DV + SL); the Fairview pendant of the Kernville terrane (KT); and Santa Lucia ("Seco") and Gabilan ("Fremont") ranges, showing the number of grains analyzed. Composite curves consist of (in parentheses): Shoo Fly complex (Lang sequence and Duncan Peak and Culbertson Lake allochthons); Roberts Mountains allochthon (Harmony, Vinini, Valmy, Snow Canyon, McAfee, Elder, and Slaven formations); Kern Plateau pendants (Bald Mountain, Indian Wells, and Kennedy pendants); Death Valley (Wood Canyon Formation and Zabriskie and Stirling quartzites); and Snow Lake terrane (Snow Lake pendant "Carrara Quartzite," "Zabriskie," "Upper Wood Canyon Formation," and "Stirling"). Colors correspond to Figure 2. Samples of unknown paleogeographic affinity shown in gray. Isotopic data in Table SD3 in the Supplemental File (see footnote 1).

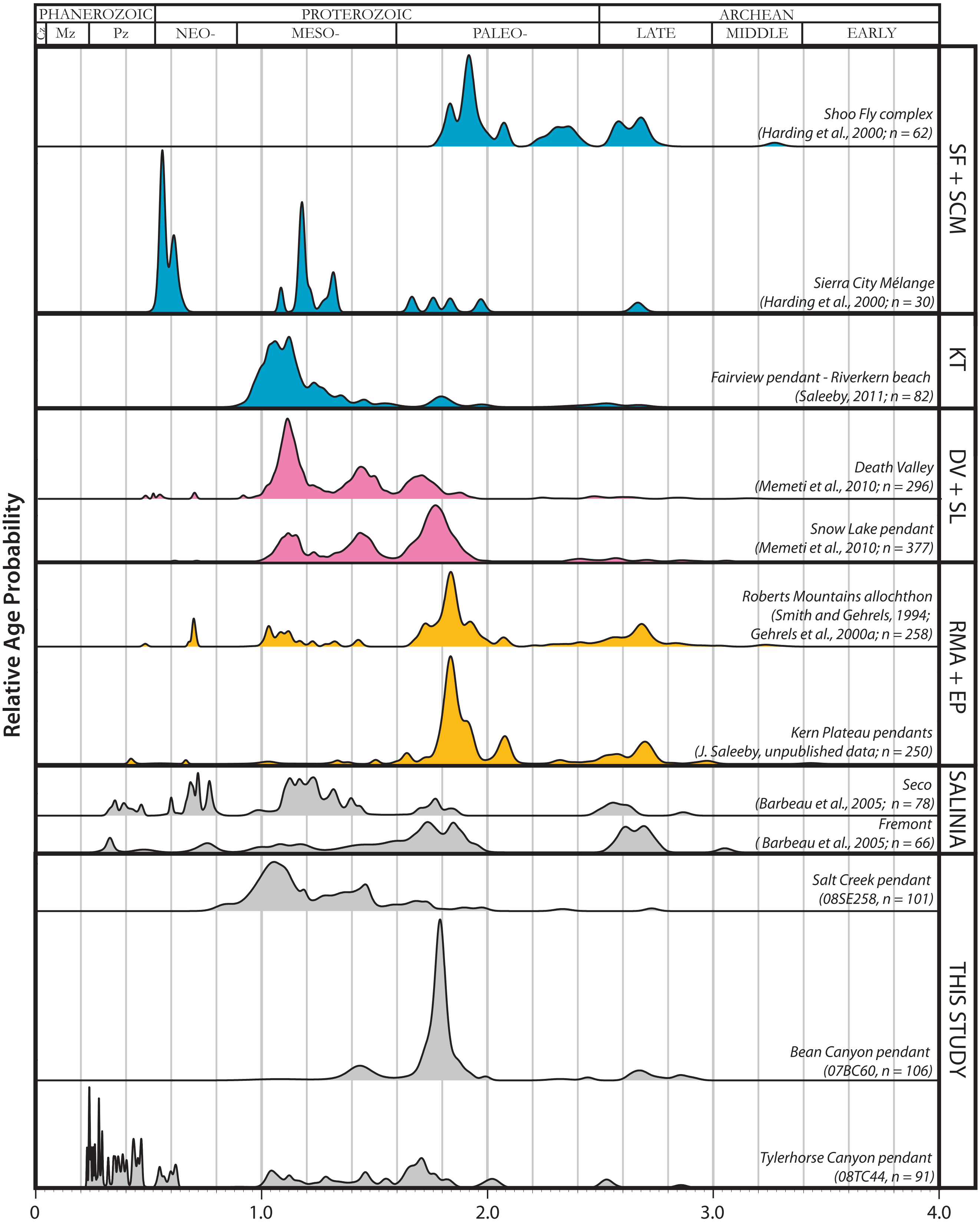
PHANEROZOIC
PROTEROZOIC
ARCHEAN
Cz
Mz
Pz
NEO-
MESO-
PALEO-
LATE
MIDDLE
EARLY
Shoo Fly complex
(Harding et al., 2000; n = 62)
Sierra City Mélange
(Harding et al., 2000; n = 30)
SF + SCM
Fairview pendant - Riverkern beach
(Saleeby, 2011; n = 82)
KT
Death Valley
(Memeti et al., 2010; n = 296)
Snow Lake pendant
(Memeti et al., 2010; n = 377)
DV + SL
Roberts Mountains allochthon
(Smith and Gehrels, 1994;
Gehrels et al., 2000a; n = 258)
Kern Plateau pendants
(J. Saleeby, unpublished data; n = 250)
RMA + EP
Seco
(Barbeau et al., 2005; n = 78)
Fremont
(Barbeau et al., 2005; n = 66)
SALINIA
Salt Creek pendant
(08SE258, n = 101)
Bean Canyon pendant
(07BC60, n = 106)
Tylerhorse Canyon pendant
(08TC44, n = 91)
THIS STUDY
Relative Age Probability
0
1.0
2.0
3.0
4.0
Age (Ga)

Figure 6.

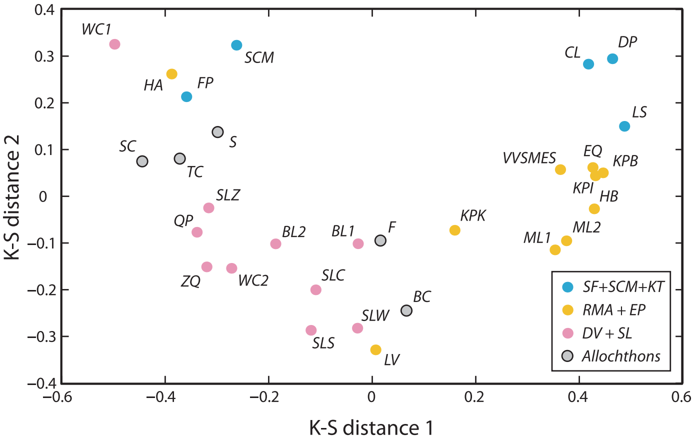

Figure 7. Multidimensional scaling map showing dimensionless Kolmogorov-Smirnov distances between arrays of detrital zircon age data. Symbol colors correspond to Figure 6. Note clustering of samples of known paleogeographic affinity. Abbreviations in key as in Figure 6. Other Abbreviations: N. and S. Sierra: CL—Culbertson Lake allochthon; DP—Duncan Peak allochthon; FP—Fairview pendant; LS—Lang sequence; SCM—Sierra City mélange (Harding et al., 2000; Saleeby, 2011). Roberts Mountains allochthon: EQ—Eureka Quartzite; HA—Harmony A; HB—Harmony B; LV—Lower Vinini; ML1—May Lake pendant (sample ML369); ML2—May Lake pendant (sample ML459); VVSMES—Upper Vinini–Valmy–Snow Canyon–McAfee-Elder-Slaven (Smith and Gehrels, 1994; Gehrels et al., 2000a; Memeti et al., 2010). El Paso terrane: KPB—Bald Mountain pendant; KPI—Indian Wells pendant; KPK—Kennedy pendant. Death Valley: WC1—Wood Canyon #1; WC2—Wood Canyon #2; ZQ—Zabriskie Quartzite (Memeti et al., 2010). Snow Lake terrane: BL1—Benson Lake pendant (sample BPM-314); BL2—Benson Lake pendant (sample RE242); QP—Quartzite Peak; SLC—Snow Lake pendant "Carrara Quartzite;" SLS—Snow Lake pendant "Stirling Quartzite;" SLW—Snow Lake pendant "Wood Canyon #2;" SLZ—Snow Lake pendant "Zabriskie" (Memeti et al., 2010). Allochthons: BC—Bean Canyon pendant; F—Fremont; S—Seco; SC—Salt Creek pendant; TC—Tylerhorse Canyon pendant (Barbeau et al., 2005; this study).

Correlation #6: Cummings Valley (F) and Salinian Framework of Montara Mountain, Northern Ben Lomond, and Bodega Head (F′)

Tonalitic plutonic rocks of Montara Mountain, northern Ben Lomond Mountain, and Bodega Head range in age from 99 to 104 Ma (James and Mattinson, 1985; James, 1992; Kistler and Champion, 2001) and have similar Sr_i (0.707–0.705) to the 99–105 Ma intrusive suite of Bear Valley (Saleeby et al., 1987; Pickett and Saleeby, 1993; Saleeby et al., 2007). Furthermore, similarities between Sur Series metasedimentary rocks of northern Salinia and the Brite Valley and Tehachapi pendants of the southern Sierra Nevada batholith (Wood, 1997) suggest that rocks found at f′ originated near Cummings Valley. Plutons and framework rocks near f′ have not received detailed thermobarometric study, although pressures of ~5 kbar are reported from metapelitic assemblages from Ben Lomond Mountain (Leo, 1967; DeCrisoforo and Cameron, 1977). Pressure determinations of 8.3–8.7 kbar are reported from the area near Cummings Valley (Pickett and Saleeby, 1993, samples GC-16 and GC-2).

Correlation #7: Southwestern Sierra Nevada Foothills (G) and Western San Emigdio Mafic Complex (G′)

Reitz (1986) suggests that the western San Emigdio mafic complex is a unique exposure of a primitive intraoceanic arc and that it does not correlate with (1) the Coast Range ophiolite because the mafic complex lacks ophiolite stratigraphy, or (2) Sierran Foothills belt peridotitic to dioritic intrusive complexes (Snoke et al., 1982) and associated ophiolitic wall rocks. This assertion is based on slight differences in

Figure 8. Photograph of probable Early Jurassic pectinid bivalve Weyla from the Tylerhorse Canyon pendant.

TABLE 2. SUMMARY OF SAMPLE LOCATIONS AND ZIRCON (U-Th)/He AGES

Sample	UTM easting*	UTM northing*	Elevation (m)	Pseudo-elevation† (m)	Mean age (Ma)	Error§ (Ma)	Number of replicates
04SS32	350708	3940938	1506	2327	77.3	8.0	4
04SS27	350384	3899048	1485	2193	72.2	4.5	4
04SS28	349061	3897426	1818	3319	83.5	6.3	4
04SS30	396529	3933080	1891	2416	70.0	3.9	3
04SS33	391015	3932556	1164	2518	76.8	2.3	4
04SS35	388629	3925972	1515	2949	84.7	6.7	6
04SS36	384771	3924533	1900	2701	69.2	2.4	4
04SS38	380280	3923122	1879	3129	78.2	8.1	5
04SS39	376370	3924106	2242	3239	73.7	5.2	4
04SS40	373067	3921963	2242	3347	76.7	5.2	4
04SS41	371086	3920961	1874	3576	83.8	5.9	5
04SS43	371523	3918853	1515	3424	81.1	8.3	7

Note: replicate data in Table SD7 in the Supplemental File (see footnote 1).
*Universal Transverse Mercator (UTM) coordinates are World Geodetic System datum, zone 11N.
†Calculated assuming apparent exhumation rate of 0.05 mm/yr; see text for discussion.
§Errors (1σ) are taken as the standard deviation divided by the square root of the number of replicates minus one.

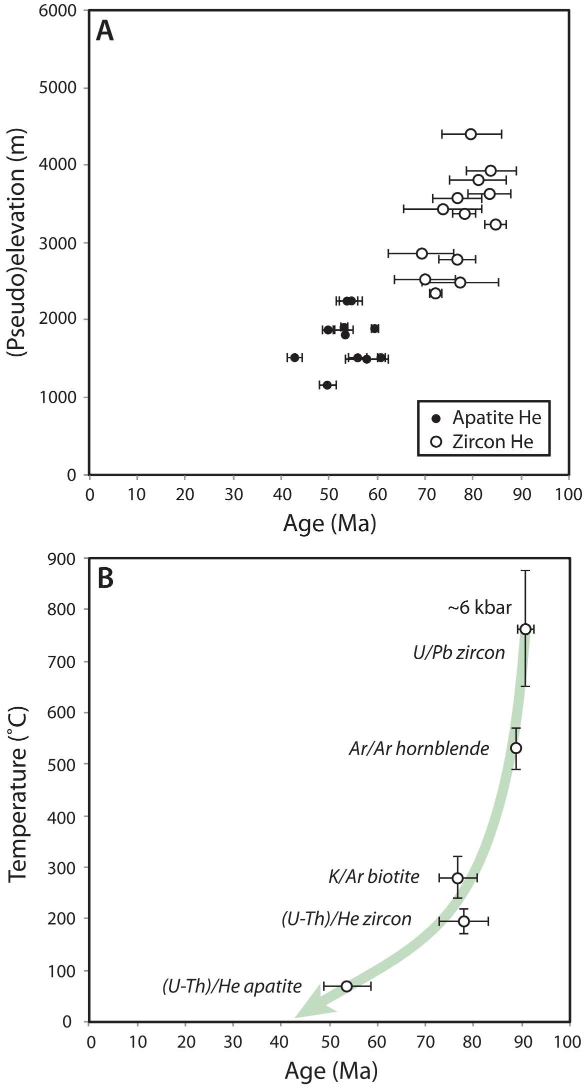

Figure 9. (A) Age elevation relationship for southern Sierra Nevada apatite (Mahéo et al., 2009) and age pseudo-elevation relationship for zircon He (this study) thermochronologic data. See text for discussion. (B) Time-temperature path for the autochthonous southern Sierra Nevada batholith. Geochronologic and thermochronometric data from Kistler and Peterman (1978), Dixon (1995), Saleeby et al. (2008), Mahéo et al. (2009), and this study.

crystallization sequence, geochemistry, and the presence of minor orthopyroxene in the western San Emigdio mafic complex, which is rare in peridotitic to dioritic complexes. New geochemical data and field relations call this interpretation into question.

Major and trace element geochemistry and $^{143}Nd/^{144}Nd$ versus $^{87}Sr/^{86}Sr$ systematics indicate that sheeted dikes and pillow basalts from the western San Emigdio mafic complex were generated through MORB magmatism (Fig. 10A). The geochemical similarity between basaltic rocks of the western San Emigdio mafic complex and the Kings-Kaweah segment of the Foothills ophiolite belt suggests that the two bodies are correlative.

Sheeted dikes and pillow basalts of the western San Emigdio mafic complex are intruded by a mid- to Late Jurassic suite of ultramafic, gabbroic, and tonalitic assemblages (Hammond, 1958; Ross, 1970, 1989; Dibblee and Nilsen, 1973; James, 1986a; Reitz, 1986) that resemble 170–150 Ma intrusive complexes of the western Sierra Nevada (Snoke et al., 1982). Zircons from tonalitic segregations in gabbros yield concordant U-Pb ages of ca. 161 Ma (James, 1986a). These gabbros are intruded by the White Ridge tonalite, which yielded a U-Pb age of 154.2 ± 3.5 Ma. Similar U-Pb zircon ages of 170–156 Ma are reported from gabbroic to tonalitic assemblages of the Mill Creek complex, which intrudes the Kings-Kaweah ophiolite belt (Saleeby and Sharp, 1980; Snoke et al., 1982; Wolf and Saleeby, 1995; Saleeby, 2011).

Exposures and basement cores of variably mylonitized and highly altered mafic to ultramafic rocks occur in the footwall of the Maricopa detachment near g (Dibblee and Chesterman, 1953; Ross, 1989; Saleeby et al., 2009a; Fig. 12A). Estimating the amount of crust that was removed by the Maricopa detachment is difficult, because the western San Emigdio mafic complex does not appear to contain assemblages conducive to thermobarometry. However, the preservation of albite-epidote and hornblende hornfels–facies assemblages in pillow basalts and sheeted dikes of the western San Emigdio mafic complex (Hammond, 1958; this study) suggest that metamorphic pressures of equilibration did not exceed ~2 kbar (Spear, 1993). Al-in-hbl pressure determinations of 4.5–5.8 kbar from footwall assemblages (Nadin and Saleeby, 2008, samples 48 and 49) suggest that restoration of g′ to g implies the removal of at least 8 km of formerly intervening crust.

Magnitude and Direction of Displacement

The correlations discussed above each imply the removal of ~5–10 km of crust along detachment faults with a north-bounding breakaway zone in the Isabella basin area. The KWF bounds the western margin of the Isabella breakaway and transfers the zone ~50 km to the

TABLE 3. SUMMARY OF THERMOBAROMETRIC CALCULATIONS FROM METAMORPHIC PENDANT ROCKS

Sample	Location	Zone	UTM easting*	UTM northing*	Mineralogy†	*T* (°C)§	*P* (kbar)§	Corr#
31001-5	Santa Lucia Mountains adjacent to the Pine Ridge ultramafic body (Bush, 1981)	10	621473	4015561	Garnet + cordierite + sillimanite + quartz	695 ± 59	3.4 ± 0.5	0.835
08TC29	Southern Tehachapi Mountains: Tylerhorse Canyon pendant	11	366844	3870569	Garnet + cordierite + andalusite + quartz + plagioclase + biotite	557 ± 40	2.4 ± 0.5	0.851
10SE41	San Emigdio Mountains: Salt Creek pendant	11	322430	3860201	Garnet + sillimanite + plagioclase + quartz	649 ± 102	3.7 ± 1.7	0.620

Note: Representative mineral compositions in Table SD8 in the Supplemental File (see footnote 1).
*Universal Transverse Mercator (UTM) coordinates are World Geodetic System datum.
†Peak equilibrium assemblages used in thermobarometric determinations.
§1σ uncertainties based on propagation of uncertainties on thermodynamic data and activity-composition relationships through thermobarometric calculations.
#Correlation coefficient between pressure and temperature from THERMOCALC.

TABLE 4. SUMMARY OF THERMOBAROMETRIC CALCULATIONS FROM PLUTONIC ROCKS

Sample	Unit	Zone	UTM easting[a]	UTM northing[a]	Hbl-Plag T[b] (°C)	Error[c]	AS95 P[d] (kbar)	Error[c]	HZ86 P[e] (kbar)	Error[c]	H87 P[f] (kbar)	Error[c]	JR89 P[g] (kbar)	Error[c]	S92 P[h] (kbar)	Error[c]
94KK27	Granodiorite of Jacobsen Meadow	11	355753	4010210	712	13 *(42)*	3.8	0.4 *(0.7)*	3.7	0.5 *(3.0)*	3.8	0.6 *(1.2)*	2.9	0.5 *(0.7)*	4.2	0.5 *(0.8)*
10SE1	Granite of Brush Mountain	11	296912	3862460	731	24 *(47)*	3.2	0.7 *(0.9)*	3.5	1.2 *(3.2)*	3.5	1.4 *(1.7)*	2.7	1.0 *(1.2)*	4.0	1.2 *(1.3)*
K16b-87	South tonalite of Vergeles	10	634652	4073302	710	8 *(41)*	4.7	0.3 *(0.7)*	4.8	0.3 *(3.0)*	5.0	0.4 *(1.1)*	3.9	0.3 *(0.6)*	5.2	0.3 *(0.7)*
04SE5	Lebec granodiorite	11	311257	3858324	636	13 *(42)*	3.3	0.9 *(1.0)*	2.6	0.9 *(3.1)*	2.5	1.0 *(1.4)*	2.0	0.7 *(0.9)*	3.1	0.8 *(1.0)*
93TH417	Claraville granodiorite	11	368657	3878458	679	15 *(43)*	3.8	0.3 *(0.7)*	3.3	0.3 *(3.0)*	3.3	0.3 *(1.1)*	2.6	0.3 *(0.6)*	3.8	0.3 *(0.7)*
91TH181	Claraville granodiorite	11	371313	3879868	732	9 *(41)*	3.6	0.3 *(0.7)*	3.9	0.2 *(3.0)*	4.0	0.3 *(1.0)*	3.1	0.2 *(0.5)*	4.4	0.2 *(0.6)*
08SE463	Tonalite of San Emigdio Creek	11	307763	3860816	711	15 *(43)*	5.2	0.6 *(0.8)*	5.2	0.5 *(3.0)*	5.5	0.5 *(1.1)*	4.2	0.4 *(0.6)*	5.7	0.4 *(0.7)*
08SE429	Tonalite of San Emigdio Creek	11	305382	3860121	687	25 *(47)*	5.6	0.3 *(0.7)*	5.4	0.3 *(3.0)*	5.7	0.3 *(1.1)*	4.4	0.2 *(0.6)*	5.8	0.3 *(0.7)*
08SE451	Antimony Peak tonalite	11	307028	3861038	675	78 *(88)*	9.7	1.5 *(1.6)*	10.0	0.4 *(3.0)*	10.9	0.4 *(1.1)*	8.2	0.3 *(0.6)*	10.2	0.3 *(0.7)*
08SE674	White Oak diorite gneiss	11	324461	3861916	657	17 *(44)*	11.0	0.3 *(0.7)*	10.6	0.1 *(3.0)*	11.5	0.1 *(1.0)*	8.8	0.1 *(0.5)*	10.7	0.1 *(0.6)*
08TC27a	Granodiorite of Gamble Spring Canyon	11	367862	3870810	626	28 *(49)*	3.0	0.6 *(0.8)*	2.2	0.5 *(3.0)*	2.1	0.6 *(1.2)*	1.7	0.5 *(0.7)*	2.8	0.5 *(0.8)*

Note: Representative mineral compositions in Tables SD9 and SD10 in the Supplemental File (see footnote 1).
[a]Universal Transverse Mercator (UTM) coordinates are World Geodetic System datum.
[b]Hornblende-plagioclase temperatures based on Holland and Blundy (1994). Calibration uncertainty: ±40 °C.
[c]1σ uncertainties based on counting statistics from multiple analyses. Overall uncertainties (in parentheses) calculated as the square root of the sum of squares of analytical and calibration errors.
[d]Anderson and Smith (1995) pressures calculated by iteration using Holland and Blundy (1994) temperatures. Calibration uncertainty: ±0.6 kbar.
[e]Hammarstrom and Zen (1986) Al-in-hbl pressures. Calibration uncertainty: ±3 kbar.
[f]Hollister et al. (1987) Al-in-hbl pressures. Calibration uncertainty: ±1 kbar.
[g]Johnson and Rutherford (1989) Al-in-hbl pressures. Calibration uncertainty: ±0.5 kbar.
[h]Schmidt (1992) Al-in-hbl pressures. Calibration uncertainty: ±0.6 kbar.

southwest to the Kern range front, the headwall for the Maricopa detachment (Figs. 1 and 12).

The average magnitude of transport is 71 ± 28 km (Table 5), calculated by measuring the map view distance between native and displaced rocks. Transport azimuths, with an average of 205 ± 28°, were determined by measuring the map view heading of the displaced site from the native site after restoring slip along San Andreas and Garlock faults. Plunge angles, with an average of 6.5 ± 3.1°, were calculated by multiplying the pressure differential between sites by 3.3 km/kbar, dividing this value by the lateral distance between sites, and taking the arc tangent of this quotient.

The determination of these values critically depends on recognizing superimposed increments of post-Cretaceous deformation that may have contributed to the transport of allochthonous fragments. The biggest challenge in "seeing through" post-Cretaceous deformation in the southern Sierra Nevada batholith and vicinity, after restoring slip along Neogene faults, is accounting for apparent clockwise vertical axis rotations of up to 90° in the region (Kanter and McWilliams, 1982; McWilliams and Li, 1983; Dokka and Ross, 1995; Wood and Saleeby, 1997; Nadin and Saleeby, 2008; Hopson et al., 2008). In short, a significant fraction of observed clockwise rotation in the southern Sierra Nevada batholith is thought to have taken place during Late Cretaceous extension (Malin et al., 1995; Saleeby, 2003; Chapman et al., 2010) and post-Cretaceous vertical axis rotation probably did not result in significant additional dispersion of upper crustal fragments in the southern Sierra Nevada batholith, with the exception of the San Emigdio Mountains, which accommodated ~7 km of north-south shortening since late Pliocene time (Davis, 1983). The reader is referred to Chapman et al. (2010) for a thorough review of rotations in the Sierran "tail."

Time-Transgressive Detachment Faulting

Integration of Al-in-hbl igneous barometry and thermochronometric data indicates that the area south of the Isabella breakaway cooled and decompressed from >650 °C and ~6 kbar (Nadin and Saleeby, 2008) at ca. 90 Ma through ~180 °C (i.e., shallow crustal levels) at 77 ± 5 Ma (Fig. 9). Such profound cooling and decompression at 77 ± 5 Ma requires a tectonic driving mechanism and is interpreted to reflect denudation related to detachment faulting along the southern Sierra detachment system at this time.

Structural data from the southern Sierra detachment system suggest, however, that detachment faulting was time-transgressive. The calculated average transport azimuth of

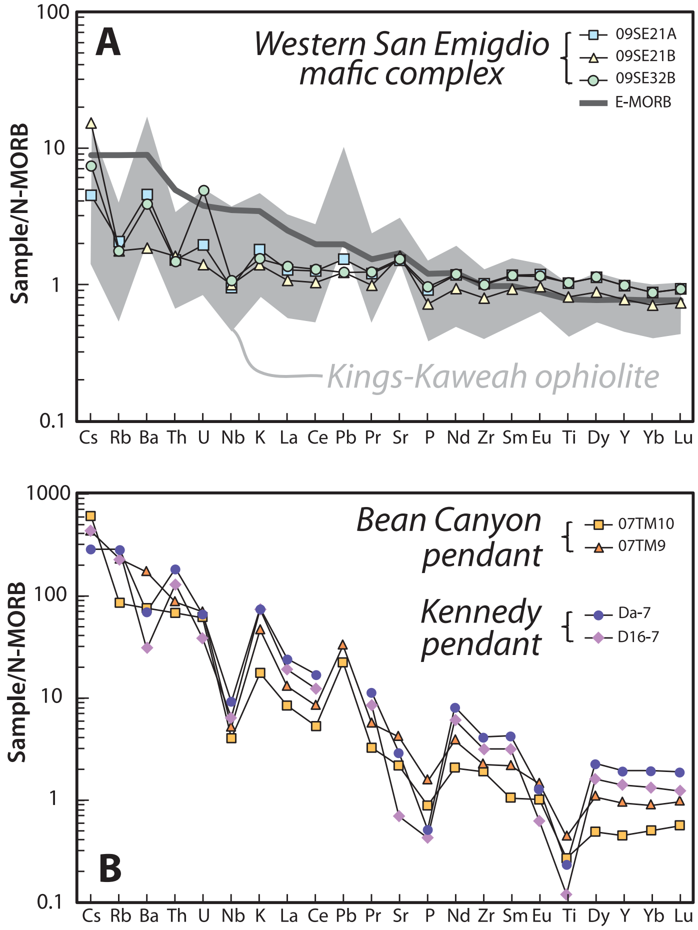

Figure 10. (A) Normal mid-ocean ridge basalt (N-MORB)–normalized trace element diagram comparing basaltic rocks of the western San Emigdio mafic complex to enriched mid-ocean ridge basalt (E-MORB) and the range of Kings-Kaweah ophiolite abundances (Saleeby, 2011). (B) N-MORB–normalized trace element diagram comparing silicic metavolcanic rocks of the Bean Canyon pendant (this study) and the Kennedy pendant of the Kern Plateau (Dunne and Suczek, 1991). Idealized N-MORB and E-MORB from Sun and McDonough (1989). Data in Table SD11 in the Supplemental File (see footnote 1).

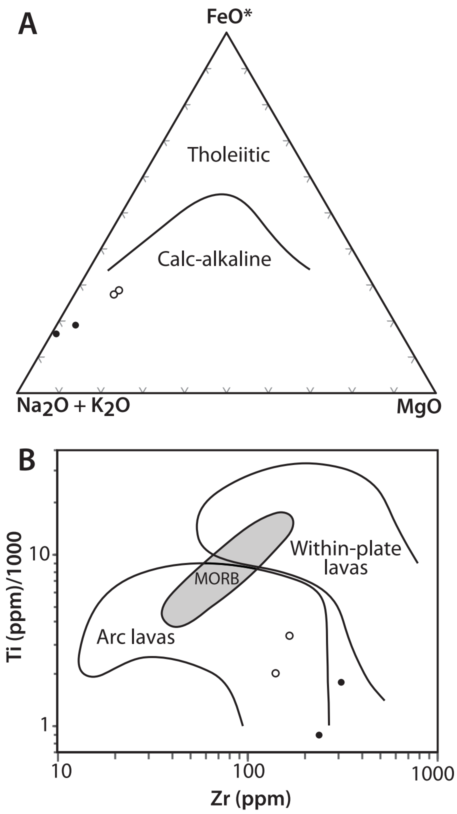

Figure 11. (A) AFM diagram showing that silicic metavolcanic rocks of the Bean Canyon pendant (open symbols) and the Kennedy pendant of the Kern Plateau (filled symbols) belong to a calc-alkaline trend. FeO* denotes total Fe as FeO. (B) Trace element discrimination diagram showing that silicic metavolcanic rocks plot within the field of arc lavas of Pearce et al. (1981). Symbols as in (A).

205 ± 28° is oblique to SSE-trending and moderately plunging lineations along the Blackburn Canyon and Jawbone Canyon faults (Wood, 1997; Wood and Saleeby, 1997) and fault II of the Rand fault complex (Nourse, 1989; Fig. 12). Two potential explanations for this difference are that Cretaceous to recent deformation has led either to remobilization of the eastern southern Sierra detachment system with a top to the SSE sense of shear, or systematic clockwise rotation of allochthonous fragments without concurrent rotation of lineations along the eastern southern Sierra detachment system. Small increments of post-Cretaceous tectonism may account for some of the discrepancy between the lineation orientation and the actual transport direction along the southern Sierra detachment system.

Our preferred explanation for the discrepancy between the lineation orientation and inferred transport direction along the southern Sierra detachment system, however, is that extension began in the southwestern Sierra Nevada batholith and propagated eastward with time. To better articulate this model, we define the following allochthonous regions of similar inferred paleogeographic affinity and timing of transport: the Logan–western San Emigdio allochthon, the northern Salinia allochthon, the Gabilan-Pastoria allochthon, the Santa Lucia allochthon, and the Jawbone-Rand allochthon (Fig. 12B). Hornblende and biotite $^{40}Ar/^{39}Ar$ and K-Ar cooling ages from the northern Salinia allochthon cluster around 90 Ma (Kistler and Champion, 2001), probably reflecting the timing of tectonic transport and upper plate attenuation from above the Cummings Valley area. The Logan–western San Emigdio allochthon was derived from a nearby area and has a similar dispersal pattern to the northern Salinia allochthon. In contrast, K-Ar hornblende and biotite ages from the Gabilan-Pastoria, Santa Lucia, and Jawbone-Rand allochthons lie in the 85 to 75 Ma range (Evernden and Kistler, 1970; Huffman, 1972), overlapping with He zircon results indicating ca. 77 Ma rapid cooling in the autochthonous southeastern Sierra Nevada batholith. We suggest that detachment and transport of these allochthons occurred at roughly 80 Ma with a more southerly transport direction than Logan–western San Emigdio and northern Salinia allochthons (Fig. 12B; Movie SD1 in the Supplemental File [see footnote 1]).

TABLE 5. SUMMARY OF CORRELATED FEATURES (SEE TEXT FOR DISCUSSION)

Correlation	Native site	Displaced site	Correlated features[a]	Approximate lateral distance between sites (km)[b]	Approximate transport azimuth[c]	Pressure differential between sites (kbar)[d]	Plunge[d,e]	Source[f]
a–a′	Area between Kern Plateau pendants and Isabella pendant	Bean Canyon and Tylerhorse Canyon pendants	S, UM, MV, DZ, IA, F, ID, Sri	100	200°	1.3–3.1	4°	This study, WS97 (b–b′)
b–b′	Erskine Canyon sequence	Oak Creek Pass complex	S, MV, IA, Sri	45	185°	0.1–3.3	7°	This study, WS97 (e–e′)
c–c′	Monolith and Back Canyon pendants	Quinn Ranch and Aqueduct Tunnel pendants	S, IA, Sri	75	220°	>1.7	4°	This study, WS97 (a–a′)
d–d′	Antelope Canyon group	Salt Creek pendant	S, DZ, IA, Sri	60	250°	2.8–3.4	10°	This study
e–e′	Area southwest of Rand Mountains	Gabilan Range, Santa Lucia Range, and southern Ben Lomond Mountain	S, UM, DZ, IA, Sri	75	225°	~2.5 (CRB)	6°	This study
f–f′	Cummings Valley	Montara Mountain, northern Ben Lomond Mountain, and Bodega Head	IA, Sri	150	250°	~3	4°	This study. WS97 (j–j′)
g–g′	Southwestern Sierra Nevada foothills	Western San Emigdio mafic complex	MV, IA, Sri	60	220°	>2.5	8°	This study
h–h′	Area between Tylerhorse Canyon and Quinn Ranch pendants	Area north of Kelso Valley	I, IA, Sri	60	210°	2.9–3.7	10°	WS97 (c–c′)
i–i′	Granite of Bob Rabbit Canyon	Granite of Tejon Lookout	I, IA, Sri	70	195°	~3	8°	WS97 (d–d′)
j–j′	Granite of Onyx	Granite of Lone Tree Canyon	I	50	170°	ND	ND	WS97 (f–f′)
k–k′	Summit gabbro of Walker Pass	Mafic plutons in the southern Rand Mountains	I	70	200°	ND	ND	WS97 (g–g′)
l–l′	Granite of Long Meadow	Granite of Bishop Ranch	I	55	160°	ND	ND	WS97 (h–h′)
m–m′	Granite of Onyx	Bishop Ranch leucogranite	I	50	185°	ND	ND	WS97 (i–i′)
Average[g]				71 ± 28	205 ± 28°	2.5 ± 0.6	6.5 ± 3.1°	

[a]DZ—Detrital zircon spectra of quartzofeldspathic intervals; F—fossils; I—igneous relations; IA—igneous ages of pendant hosting plutons; ID—independence dikes present; MV—presence of metavolcanics of similar geochemistry and age; S—stratigraphic relations; Sri—Sri of pendant hosting plutons; UM—presence of geochemically enriched ultramafic rock.
[b]Calculated by measuring the map view distance between native and displaced sites after restoring slip along San Andreas and Garlock faults.
[c]Calculated by measuring the map view heading of the displaced site from the native site after restoring slip along San Andreas and Garlock faults.
[d]CRB—Coast Ridge belt; ND—not determined.
[e]Calculated by multiplying the pressure differential between sites by 3.3 km/kbar, dividing this value by the lateral distance between sites, and taking the arc tangent of this quotient.
[f]WS97—Letters in parentheses correspond to correlations inferred by Wood and Saleeby (1997).
[g]1σ uncertainties based on counting statistics from multiple measurements.

A similar outboard to inboard time-transgressive model invoking oblique collision of an aseismic ridge with North America is envisioned by Barth and Schneiderman (1996) and Chapman et al. (2010) to explain an ~20 Myr time lag in schist cooling ages between the southwestern Sierra Nevada batholith, northwestern Mojave Desert, and Salinia. We speculate that south- and SSE-directed transport of upper crustal fragments in the Jawbone-Rand allochthon resulted as schist eduction created a void at the lateral ramp in the subduction megathrust, approximately centered along the trace of the superimposed Garlock fault, causing superjacent batholithic crust to breach southward across the inflection zone (Fig. 13).

Late Cretaceous Gravitational Collapse of the Southern Sierra Nevada Batholith

A thorough review of crosscutting relationships between dated plutons, detachment faults, and Late Cretaceous to Eocene nonconformities by Wood and Saleeby (1997) loosely brackets tectonic unroofing along the southern Sierra detachment system and the transport of upper crustal fragments to between ca. 90 and 50 Ma, suggesting that extension may have taken place over as much as 40 Myr. However, thermochronometric work presented here and a recent review of available geochronologic, thermochronometric, and thermobarometric data (Chapman et al., 2010) indicate that the majority of extension, while diachronous across the southern Sierra Nevada, occurred entirely within the Late Cretaceous.

The transport of upper crustal fragments from above the southern Sierra Nevada batholith at 77 ± 5 Ma coincides with: (1) structural ascent of deep batholithic rocks in the Tehachapi, San Emigdio, Santa Lucia, and Rand Mountains from ca. 95 to 70 Ma (Malin et al., 1995; Fletcher et al., 2002; Kidder et al., 2003; Saleeby et al., 2007); (2) rapid eduction of the schist from beneath the autochthon from ca. 90 to 70 Ma (Barth et al., 2003; Grove et al., 2003; Kidder and Ducea, 2006; Chapman et al., 2010); (3) dextral strike-slip transfer motion along the KWF (Nadin and Saleeby, 2008); (4) dextral shear across Owens Valley (Bartley et al., 2007); and (5) marine transgression and deposition of supradetachment basin deposits across the highly attenuated crust of the southern Sierra Nevada batholith and adjacent areas (Grove, 1993; Wood and Saleeby, 1997; Saleeby, 2003).

Structural and kinematic relations from the Rand fault and Salinas shear zone suggest that the schist moved from deep to shallow crustal levels with a lower plate to the SSW (210 ± 10°)

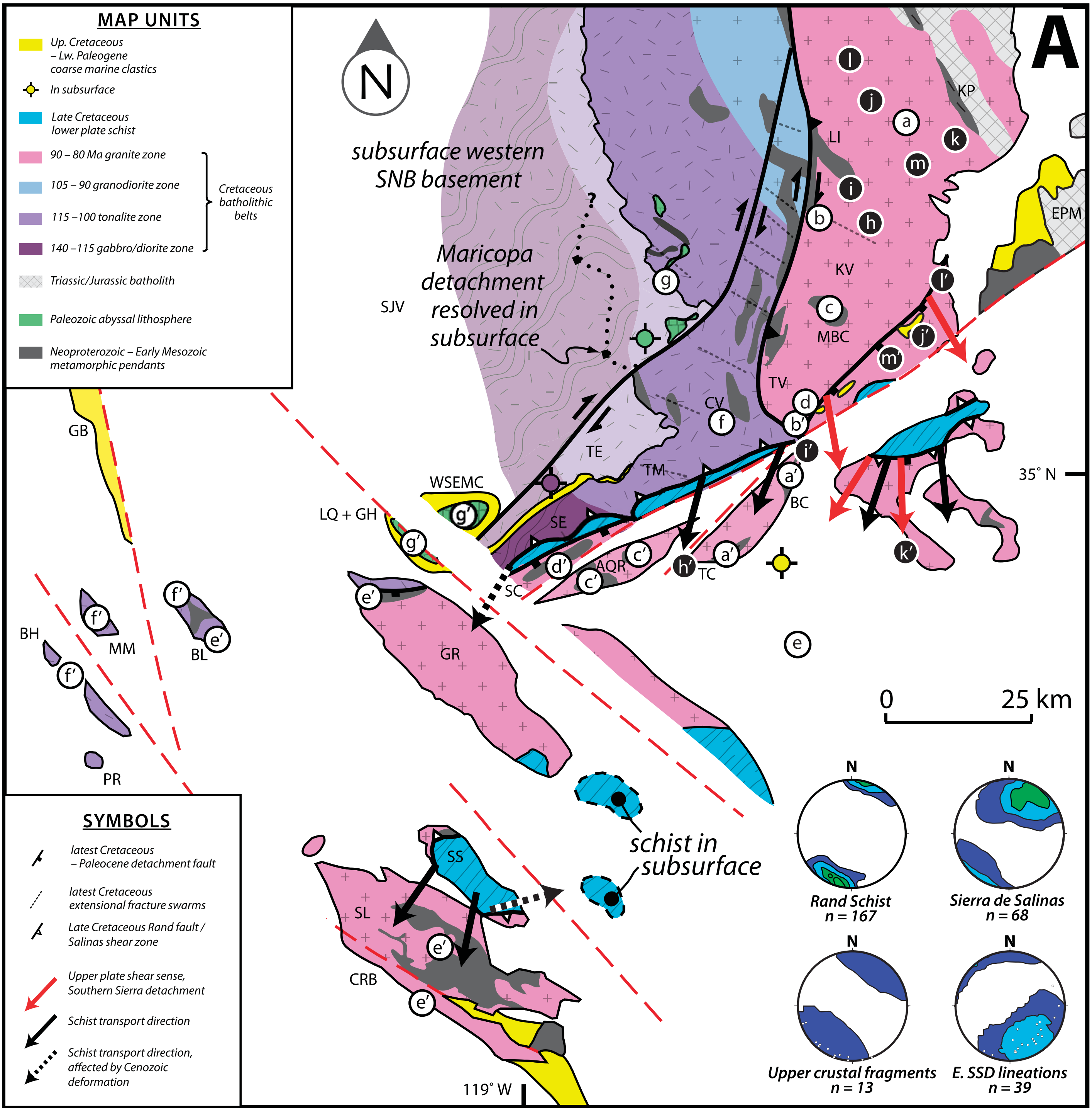

Figure 12 (*on this and following page*). **(A) Tectonic map of Figure 1 with Pliocene–Quaternary north-south shortening in the San Emigdio Mountains (Davis, 1983) removed and inferred allochthon (primed letters)-autochthon (corresponding letters) correlations and kinematic relations overlain. Correlations of Wood and Saleeby (1997) shown as black circles. Correlations of this study shown as white circles. Schist and allochthonous plate shear sense determinations from Nourse (1989), Wood and Saleeby (1997), and Chapman et al. (2010). Equal-area lower-hemisphere stereonets show lineation measurements from the Rand Schist (Postlethwaite and Jacobson, 1987), schist of Sierra de Salinas (Chapman et al., 2010), the southern Sierra detachment, and inferred transport directions of upper crustal fragments (Kamb contour interval 4σ; Table 5). Abbreviations, symbols, and map units as in Figures 1 and 2.**

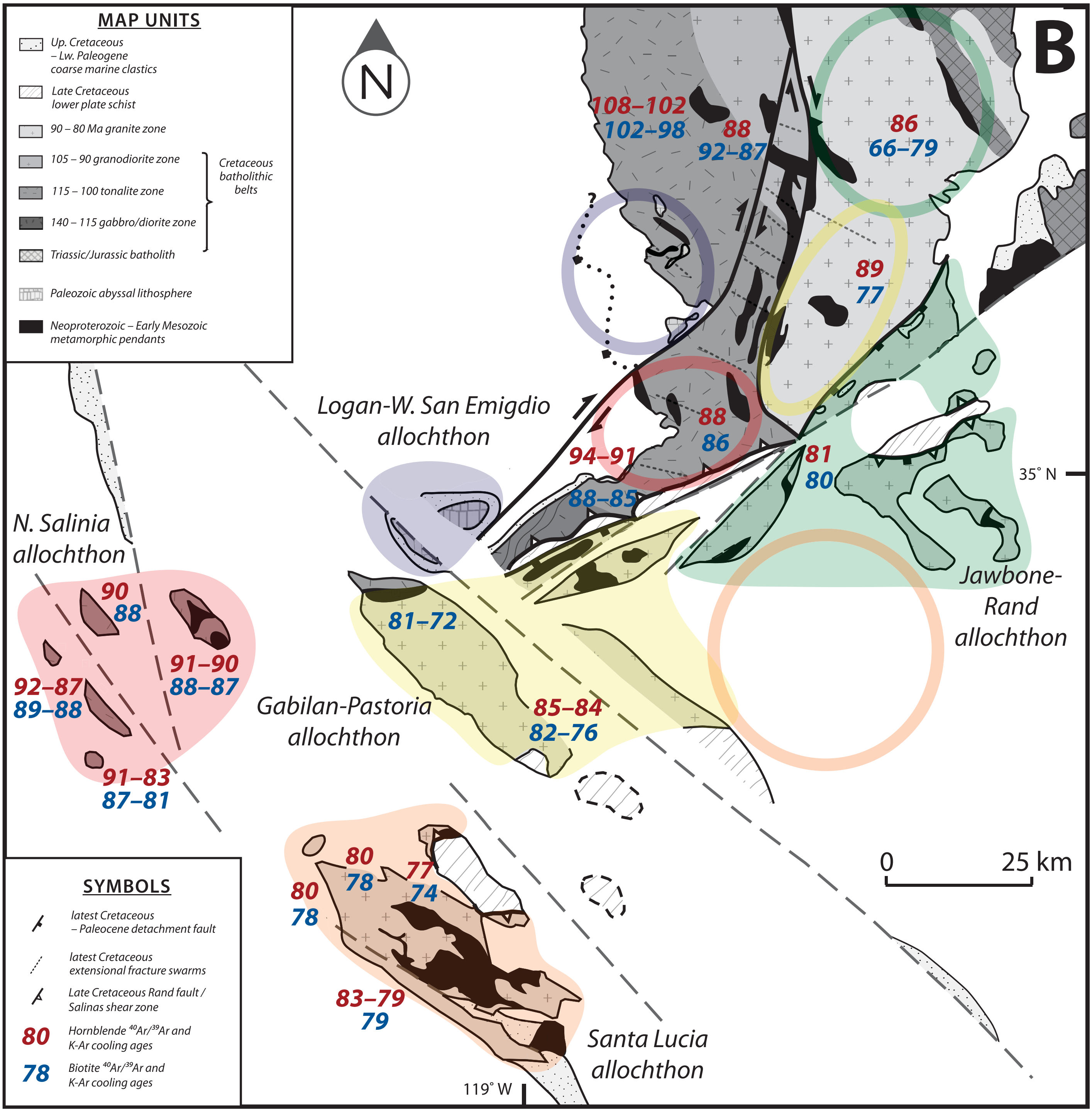

Figure 12 (*continued*). (B) Map showing allochthonous regions of similar inferred paleogeographic affinity (shaded), correlative autochthonous areas (outlined with corresponding colors), and $^{40}Ar/^{39}Ar$ and K-Ar cooling ages (Evernden and Kistler, 1970; Huffman, 1972; Ross, 1989; Kistler and Champion, 2001; Saleeby et al., 2007). An accompanying animation can be found in Movie SD1 in the Supplemental File (see footnote 1). Abbreviations, symbols, and map units as in Figures 1 and 2.

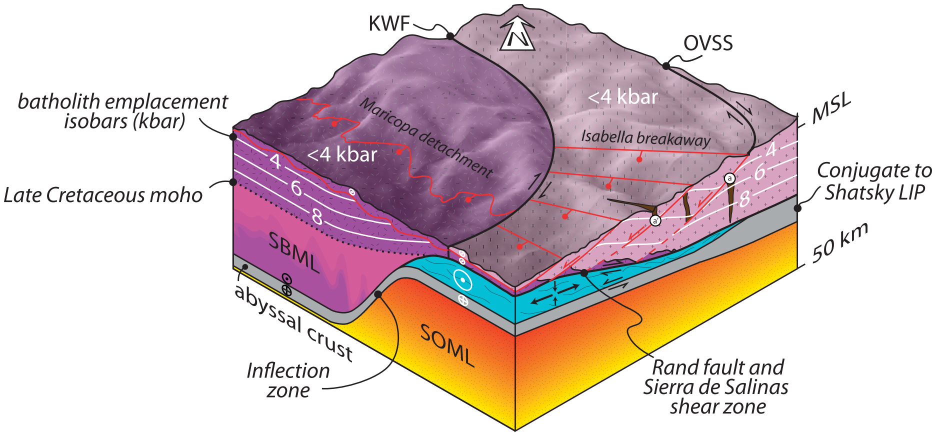

Figure 13. Tectonic model for Late Cretaceous free-boundary gravitational collapse and transport of upper crustal fragments in the southern Sierra Nevada batholith. Strain coupling between the schist (shown in blue) and upper plates accompanies high magnitude extension and lateral spreading toward the unconfined continental margin. Displaced pendant with vertical piercing point (a–a′) shown in brown. Abbreviations: KWF—Late Cretaceous Kern Canyon–White Wolf fault system; LIP—large igneous province; MSL—mean sea level; OVSS—Owens Valley shear system; SBML—sub-batholith mantle lithosphere; SOML—sub-oceanic mantle lithosphere.

sense of shear (Chapman et al., 2010), overlapping with the 205 ± 28° transport direction of allochthonous upper crustal assemblages (Fig. 12). These relations indicate that coeval SSW-directed transport of the entire crustal column, from upper plate shallow-level assemblages of the southern Sierra Nevada batholith, Mojave Desert, and Salinian block, through middle plate deep-crustal exposures of the southern Sierra Nevada batholith, and into the lower plate schist, occurred in Late Cretaceous time. Late Cretaceous trenchward flow of Rand and related schists (Malin et al., 1995; Saleeby, 2003; Chapman et al., 2010) and strain coupling between the educting schist and upper plate(s) provide an explanation for the overlapping transport directions along the southern Sierra detachment system, Rand fault, and Salinas shear zone. We speculate that strain coupling between the schist and deep batholithic plate along the Rand fault and Salinas shear zone and, in turn, between the deep batholithic plate and upper crustal fragments along the southern Sierra detachment system, reflects gravitational collapse of the southern Sierra Nevada batholith and adjacent northwest Mojave and Salinia.

Mass transfer associated with lateral spreading and vertical thinning of the Sierran crust leads to a space problem. Rey et al. (2001) address this space problem by defining two end-member modes of gravitational collapse in which gravitational potential energy is (“fixed-boundary collapse”) and is not (“free-boundary collapse”) transferred from hinterland to foreland regions. South- to southwestward-directed extension of the entire crustal column of the southern Sierra Nevada batholith without synchronous shortening in the foreland best fits the criteria for free-boundary gravitational collapse. However, Late Cretaceous transcurrent faulting along the KWF and Owens Valley shear system has partitioned the highly extended and exhumed core of the southern Sierra Nevada batholith from less extended and exhumed adjacent regions. These relations imply that SSW-directed extrusion toward the unconfined continental margin probably accompanied crustal attenuation in the southern Sierra Nevada batholith (Fig. 13). Subduction of a LIP beneath the southern Sierra Nevada batholith and adjacent areas (Liu et al., 2010) and associated transient horizontal compressional stresses, basal shear stresses, and lithospheric strength (i.e., the replacement of mantle wedge material with underplated schist) is posited to have preconditioned the southern Sierra Nevada batholith for lateral extrusion-modified, free-boundary collapse.

Southern Sierra Landscape Development

Apatite He data (Mahéo et al., 2009) from the zircon He sample suite can be further utilized to approximate the position of the southern Sierra detachment system surface relative to the modern topographic surface and to relate the topography of the detachment surface to the early landscape development of the greater Sierra Nevada. Following the termination of large volume arc magmatism in the Sierra Nevada batholith at ca. 84 Ma (Chen and Moore, 1982), the topographic surface of the arc underwent slow regional erosion at a rate of 0.05 ± 0.01 mm/yr throughout much of Cenozoic time (Clark et al., 2005; Cecil et al., 2006; Mahéo et al., 2009). Thus the constructional topographic surface of the greater Sierran arc, commonly interpreted to have constituted the western margin of a Cordilleran-wide orogenic plateau locally termed the Nevadaplano (DeCelles, 2004), began to slowly erode at virtually the same time as the tectonically denuded lower plate regime of the southern Sierra detachment system.

Apatite He age-elevation relations are used to adjust each data point of our zircon He suite to a position (“virtual distance”) that would correspond to the freshly denuded detachment surface (Fig. 14). The reconstructed detachment surface is subhorizontal and projects at ~2 ± 1 km above the modern landscape. We have also calculated “virtual pressures” of igneous equilibration by dividing calculated “virtual distances” by 3.3 km/kbar and adding this quotient to existing Al-in-hbl pressure determinations, where available. Calculated “virtual pressures” reveal the crustal depth of the footwall of the southern Sierra detachment system at the moment of large magnitude detachment faulting.

Figure 14 shows that the detachment surface in the area of the sample traverse sat at ~4 ± 1 kb levels of the crust, which corresponds well to the typical 3 ± 1 kb crustal levels determined for the allochthons. These features are synthesized in Figure 15, a regional N-S cross section crossing the restored Rand Mountains, extending the schist under the southern Sierra Nevada batho-

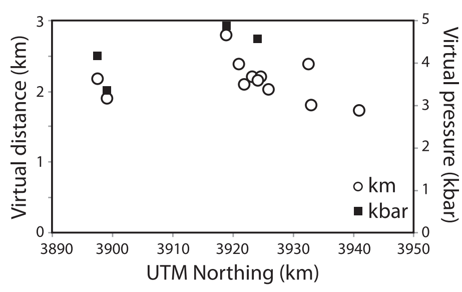

Figure 14. Plot showing “virtual distance,” the calculated distance above the modern landscape of the reconstructed detachment surface, versus northing. Secondary axis shows “virtual pressure” of igneous equilibration, calculated along the reconstructed detachment fault, for locations where Al-in-hbl determinations are available (samples 04SS27, 04SS28, 04SS39, and 04SS43 of Nadin and Saleeby, 2008). See text for discussion.

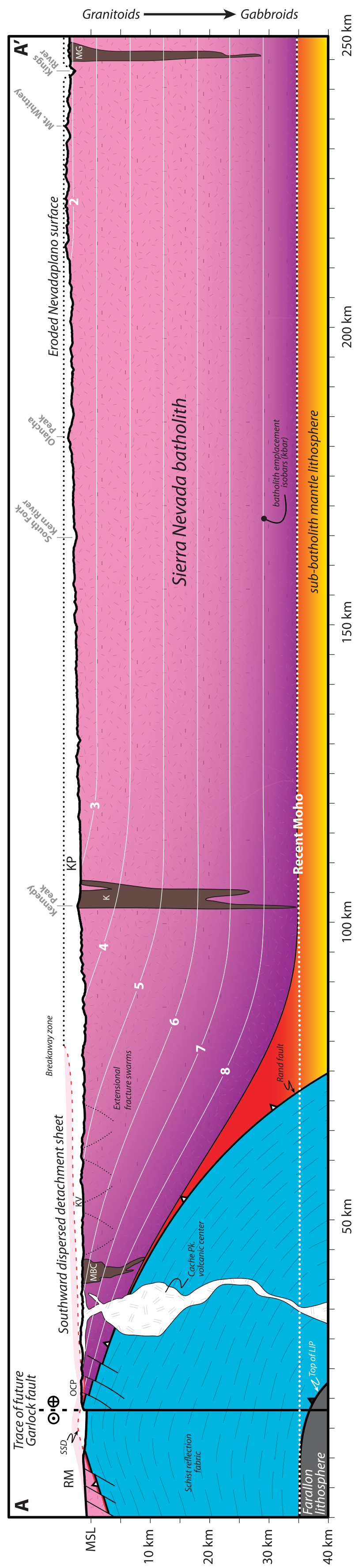

Figure 15. Regional geologic cross section from the Rand Mountains to the Nevadaplano margin. Note that the reconstructed detachment surface merges with the Nevadaplano surface at the Isabella breakaway. Cross-section trace shown in Figure 1. Abbreviations, symbols, and map units as in Figure 1. Other abbreviations: LIP—Large igneous province; MSL—mean sea level; SSD—southern Sierra detachment system.

lith, and passing north of footwall assemblages of the southern Sierra detachment system, with the system continuing northward as the reconstructed detachment surface up to the Isabella breakaway zone. The breakaway zone ramps up to the Kern plateau and continues to the Nevadaplano margin with the Late Cretaceous–early Tertiary paleodrainage of the Kings River region shown at the northern end of the section (House et al., 2001; Saleeby et al., 2009b). This cross section represents a snapshot of southern Sierra paleolandscape and large-scale crustal structure immediately following large-magnitude detachment faulting.

CONCLUSIONS

Integration of new field and structural relations, U-Pb zircon geochronology, thermobarometry, major and trace element chemistry, Sr and Nd isotopic ratios, and zircon (U-Th)/He thermochronometry with existing databases reveals temporal and spatial overlap between: (1) tectonic transport of allochthonous fragments of shallow-level eastern Sierra Nevada batholith affinity rocks; (2) structural attenuation and ascent of deep-level western Sierra Nevada batholith assemblages; and (3) trench-directed flow in the schist. These relationships suggest that the entire crustal column of the southern Sierra Nevada batholith and vicinity collapsed in Late Cretaceous time due to excess gravitational potential energy.

This work places several constraints on the timing and magnitude of extension attending gravitational collapse of the southern Sierra Nevada batholith. First, zircon (U-Th)/He data presented herein reveal a rapid cooling event at 77 ± 5 Ma, probably reflecting the time of large-magnitude detachment faulting in the southern Sierra Nevada batholith autochthon. A comparison of this data set with existing apatite (U-Th)/He thermochronometry from the same sample suite (Mahéo et al., 2009) suggests that the development of modern landscape and arrangement of tectonic elements in southern California was greatly preconditioned by Late Cretaceous tectonics. Most notably is the southward-sloping topographic gradient off the modern southern Sierra, which reflects elevation loss in that region due to extension and detachment faulting. Second, palinspastic restoration of seven presumably correlative allochthon-autochthon pairs implies 50–70 km of lateral transport and the removal of ~5–10 km of crust along the southern Sierra detachment system. Finally, the timing and the kinematics of dispersal of upper crustal fragments and ascent of deep-level batholithic and subduction accretion assemblages overlap, suggesting that the shallow and deep crust were highly coupled during gravitational collapse. The observations presented here clarify several issues pertaining to Late Cretaceous orogenesis and subsequent collapse of the southern Sierra Nevada batholith and vicinity, and are consistent with the free-boundary gravitational collapse mode of Rey et al. (2001).

ACKNOWLEDGMENTS

This research was supported by National Science Foundation grant EAR-0739071 and by the Gordon and Betty Moore Foundation. This is Caltech Tectonics Observatory Contribution 188. The manuscript benefitted from enlightening discussions with M. Robinson Cecil, George Dunne, Vali Memeti, Elisabeth Nadin, and Scott Paterson and from thoughtful reviews by Jade Star Lackey, John Bartley, and Associate Editor Keith Putirka. We thank Pieter Vermeesch for providing a MATLAB script for multidimensional scaling of U-Pb detrital zircon ages. Ronald Kistler graciously provided samples of north and south tonalites of Vergeles (Gabilan Range).

REFERENCES CITED

Ague, J.J., 1997, Thermodynamic calculation of emplacement pressures for batholithic rocks, California: Implications for the aluminum-in-hornblende barometer: Geology, v. 25, no. 6, p. 563–566, doi:10.1130/0091-7613(1997)025<0563:TCOEPF>2.3.CO;2.

Ague, J.J., and Brimhall, G.H., 1988, Magmatic arc asymmetry and distribution of anomalous plutonic belts in the batholiths of California: Effects of assimilation, crustal thickness, and depth of crystallization: Geological Society of America Bulletin, v. 100, no. 6, p. 912–927, doi:10.1130/0016-7606(1988)100<0912:MAADO>2.3.CO;2.

Anderson, J.L., and Smith, D.R., 1995, The effects of temperature and fO_2 on the Al-in-hornblende barometer: The American Mineralogist, v. 80, no. 5–6, p. 549–559.

Barbeau, D.L., Ducea, M.N., Gehrels, G.E., Kidder, S., Wetmore, P.H., and Saleeby, J.B., 2005, U-Pb detrital-zircon geochronology of northern Salinian basement and cover rocks: Geological Society of America Bulletin, v. 117, no. 3, p. 466–481, doi:10.1130/B25496.1.

Barth, A.P., and Schneiderman, J.S., 1996, A comparison of structures in the Andean orogen of northern Chile and exhumed midcrustal structures in southern California, USA: An analogy in tectonic style?: International Geology Review, v. 38, no. 12, p. 1075–1085, doi:10.1080/00206819709465383.

Barth, A.P., Wooden, J.L., Grove, M., Jacobson, C.E., and Pedrick, J.N., 2003, U-Pb zircon geochronology of rocks in the Salinas Valley region of California: A reevaluation of the crustal structure and origin of the Salinian Block: Geology, v. 31, no. 6, p. 517–520, doi:10.1130/0091-7613(2003)031<0517:UZGORI>2.0.CO;2.

Bartley, J.M., Glazner, A.F., Coleman, D.S., Kylander-Clark, A.R.C., and Friedrich, A.M., 2007, Large Laramide dextral offset across Owens Valley, California, and its possible relation to tectonic unroofing of the southern Sierra Nevada, *in* Till, A.B., Roeske, S.M., Foster, D.A. and Sample, J.C., eds., Exhumation Processes along Major Continental Strike-Slip Fault Systems: Geological Society of America Special Paper 434, p. 129–148.

Bush, R.N., 1981, Small Salinian ultramafic bodies near Jamesburg, California [M.S. thesis]: Stanford University, 123 p.

Carl, B.S., and Glazner, A.F., 2002, Extent and significance of the Independence dike swarm, eastern California, *in* Glazner, A.F., Walker, J.D., and Bartley, J.M., eds., Geologic Evolution of the Mojave Desert and Southwestern Basin and Range: Geological Society of America Memoir 195, p. 117–130.

Carr, M.D., Christiansen, R.L., and Poole, F.G., 1984, Pre-Cenozoic geology of the El Paso Mountains, southwestern Great Basin, California—Summary, *in* Lintz, J.J., ed., Western Geological Excursions, v. 4: Reno, Nevada, Macleay School of Mines, p. 84–93.

Cecil, M.R., Ducea, M.N., Reiners, P.W., and Chase, C.G., 2006, Cenozoic exhumation of the northern Sierra Nevada, California, from (U-Th)/He thermochronology: Geological Society of America Bulletin, v. 118, no. 11–12, p. 1481–1488, doi:10.1130/B25876.1.

Chapman, A.D., and Saleeby, J., 2012, Geologic map of the San Emigdio Mountains: Geological Society of America Map and Chart Series, v. MCH-101, 1:40,000 scale.

Chapman, A.D., Kidder, S., Saleeby, J.B., and Ducea, M.N., 2010, Role of extrusion of the Rand and Sierra de Salinas schists in Late Cretaceous extension and rotation of the southern Sierra Nevada and vicinity: Tectonics, v. 29, doi:10.1029/2009TC002597.

Chapman, A.D., Luffi, P., Saleeby, J., and Petersen, S., 2011, Metamorphic evolution, partial melting, and rapid exhumation above an ancient flat slab: Insights from the San Emigdio Schist, southern California: Journal of Metamorphic Geology, v. 29, p. 601–626, doi:10.1111/j.1525-1314.2011.00932.x.

Cheadle, M.J., Czuchra, B.L., Byrne, T., Ando, C.J., Oliver, J.E., Brown, L.D., Kaufman, S., Malin, P.E., and Phinney, R.A., 1986, The deep crustal structure of the Mojave Desert, California, from COCORP seismic reflection data: Tectonics, v. 5, p. 293–320, doi:10.1029/TC005i002p00293.

Chen, J.H., and Moore, J.G., 1979, Late Jurassic Independence dike swarm in eastern California: Geology, v. 7, no. 3, p. 129–133, doi:10.1130/0091-7613(1979)7<129:LJIDSI>2.0.CO;2.

Chen, J.H., and Moore, J.G., 1982, Uranium-lead isotopic ages from the Sierra Nevada batholith, California: Journal of Geophysical Research, v. 87, p. 4761–4784, doi:10.1029/JB087iB06p04761.

Clark, M.K., Mahéo, G., Saleeby, J., and Farley, K.A., 2005, The non-equilibrium landscape of the southern Sierra Nevada, California: GSA Today, v. 15, no. 9, p. 4–10, doi:10.1130/1052-5173(2005)015[4:TNLOTS]2.0.CO;2.

Critelli, S., and Nilsen, T.H., 2000, Provenance and stratigraphy of the Eocene Tejon Formation, Western Tehachapi Mountains, San Emigdio Mountains, and southern San Joaquin Basin, California: Sedimentary Geology, v. 136, no. 1–2, p. 7–27, doi:10.1016/S0037-0738(00)00080-4.

Crowell, J.C., 1952, Geology of the Lebec Quadrangle, California: Special Report, California Division of Mines and Geology, v. 24, p. 1–24.

Davis, T.L., 1983, Late Cenozoic structure and tectonic history of the western "Big Bend" of the San Andreas fault and adjacent San Emigdio Mountains [Ph.D. thesis]: University of California, Santa Barbara, 563 p.

DeCelles, P.G., 2004, Late Jurassic to Eocene evolution of the Cordilleran thrust belt and foreland basin system, western U.S: American Journal of Science, v. 304, no. 2, p. 105–168, doi:10.2475/ajs.304.2.105.

DeCrisoforo, D.T., and Cameron, K.L., 1977, Petrology of sillimanite-K-spar zone metapelites from Ben Lomond Mountain, central Coast Ranges, California: Geological Society of America Abstracts with Programs, v. 9, p. 411.

Dewey, J.F., 1988, Extensional collapse of orogens: Tectonics, v. 7, p. 1123–1139, doi:10.1029/TC007i006p01123.

Dibblee, T.W., Jr., and Chesterman, C.W., 1953, Geology of the Breckenridge Mountain Quadrangle, California: California Division of Mines and Geology Bulletin, v. 168, p. 1–56.

Dibblee, T.W., Jr., and Nilsen, T.H., 1973, Geologic map of San Emigdio and western Tehachapi Mountains, *in* Vedder, J.G., ed., Sedimentary Facies Changes in Tertiary Rocks—California Transverse and Southern Coast Ranges: Anaheim, California: Society of Economic Paleontologists and Mineralogists Guidebook to Field Trip 2.

Dickinson, W.R., Ducea, M., Rosenberg, L.I., Greene, H.G., Graham, S.A., Clark, J.C., Weber, G.E., Kidder, S., Ernst, G.W., and Brabb, E.E., 2005, Net dextral slip, Neogene San Gregorio-Hosgri fault zone, coastal California: Geologic evidence and tectonic implications: Geological Society of America Special Paper 391, 43 p.

Dixon, E.T., 1995, $^{40}Ar/^{39}Ar$ hornblende geochronology and evaluation of garnet and hornblende barometry, Lake Isabella, the Tehachapi area, southern Sierra Nevada, California [M.S. thesis]: University of Michigan, 63 p.

Dokka, R.K., and Ross, T.M., 1995, Collapse of southwestern North America and the evolution of early Miocene detachment faults, metamorphic core complexes, the Sierra Nevada orocline, and the San Andreas fault system: Geology, v. 23, no. 12, p. 1075–1078, doi:10.1130/0091-7613(1995)023<1075:COSNAA>2.3.CO;2.

Ducea, M.N., and Saleeby, J.B., 1998, The age and origin of a thick mafic-ultramafic keel from beneath the Sierra Nevada Batholith: Contributions to Mineralogy and Petrology, v. 133, p. 169–185, doi:10.1007/s004100050445.

Ducea, M.N., Kidder, S., Chelsey, J.T., and Saleeby, J.B., 2009, Tectonic underplating of trench sediments beneath magmatic arcs, the central California example: International Geology Review, v. 51, p. 1–26, doi:10.1080/00206810802602767.

Dunne, G.C., and Suczek, C.A., 1991, Early Paleozoic eugeoclinal strata in the Kern Plateau pendants, southern Sierra Nevada, California, *in* Cooper, J.D., and Stevens, C.H., eds., Paleozoic Paleogeography of the Western United States: Pacific Section, Society of Economic Paleontologists and Mineralogists, v. 2, p. 677–692.

Ehlig, P.L., 1981, Origin and tectonic history of the basement terrane of the San Gabriel Mountains, central Transverse Ranges, *in* Ernst, W.G., ed., The Geotectonic Development of California, Rubey Volume I: New Jersey, Prentice-Hall, p. 253–283.

Evernden, J.F., and Kistler, R.W., 1970, Chronology of emplacement of Mesozoic batholithic complexes in California and western Nevada: U.S. Geological Survey Professional Paper 623, 42 p.

Fletcher, J.M., Miller, J.S., Martin, M.W., Boettcher, S.S., Glazner, A.F., and Bartley, J.M., 2002, Cretaceous arc tectonism in the Mojave Block: Profound crustal modification that controlled subsequent tectonic regimes: Geological Society of America Memoir 195, p. 131–149.

Gehrels, G.E., Dickinson, W.R., Riley, B.C.D., Finney, S.C., and Smith, M.T., 2000a, Detrital zircon geochronology of the Roberts Mountains allochthon, Nevada: Geological Society of America Special Paper 347, p. 19–42.

Gehrels, G.E., Dickinson, W.R., Darby, B.J., Harding, J.P., Manuszak, J.D., Riley, B.C.D., Spurlin, M.S., Finney, S.C., Girty, G.H., Harwood, D.S., Miller, M.M., Satterfield, J.I., Smith, M.T., Snyder, W.S., Wallin, E.T., and Wyld, S.J., 2000b, Tectonic implications of detrital zircon data from Paleozoic and Triassic strata in western Nevada and Northern California: Geological Society of America Special Paper 347, p. 133–150.

Glazner, A.F., Walker, J.D., and Bartley, J.M., 1989, Magnitude and significance of Miocene crustal extension in the central Mojave Desert, California: Geology, v. 17, p. 50–53, doi:10.1130/0091-7613(1989)017<0050:MASOMC>2.3.CO;2.

Glazner, A.F., Bartley, J.M., Ingersoll, R.V., Dokka, R.K., and Ross, T.M., 1996, Collapse of southwestern North America and the evolution of early Miocene detachment faults, metamorphic core complexes, the Sierra Nevada orocline, and the San Andreas fault system: Comment and Reply: Geology, v. 24, p. 858–859, doi:10.1130/0091-7613(1996)024<0858:COSNAA>2.3.CO;2.

Glazner, A.F., Walker, J.D., Bartley, J.M., and Fletcher, J.M., 2002, Cenozoic evolution of the Mojave block and environs, *in* Glazner, A.F., Walker, J.D., and Bartley, J.M., eds., Geologic Evolution of the Mojave Desert and Southwestern Basin and Range: Geological Society of America 195, p. 19–41.

Graham, C.M., and England, P.C., 1976, Thermal regimes and regional metamorphism in the vicinity of overthrust faults: An example of shear heating and inverted metamorphic zonation from southern California: Earth and Planetary Science Letters, v. 31, no. 1, p. 142–152, doi:10.1016/0012-821X(76)90105-9.

Grasse, S.W., Gehrels, G.E., Lahren, M.M., Schweickert, R.A., and Barth, A.P., 2001, U-Pb geochronology of detrital zircons from the Snow Lake Pendant, central Sierra Nevada; implications for Late Jurassic–Early Cretaceous dextral strike-slip faulting: Geology, v. 29, no. 4, p. 307–310, doi:10.1130/0091-7613(2001)029<0307:UPGODZ>2.0.CO;2.

Grove, K., 1993, Latest Cretaceous basin formation within the Salinian Terrane of west-central California: Geological Society of America Bulletin, v. 105, no. 4, p. 447–463, doi:10.1130/0016-7606(1993)105<0447:LCBFWT>2.3.CO;2.

Grove, M., Jacobson, C.E., Barth, A.P., and Vucic, A., 2003, Temporal and spatial trends of Late Cretaceous–early Tertiary underplating Pelona and related schist beneath southern California and southwestern Arizona: Geological Society of America Special Paper 374, p. 381–406.

Hammarstrom, J.M., and Zen, E.A., 1986, Aluminum in hornblende: An empirical igneous geobarometer: The American Mineralogist, v. 71, no. 11–12, p. 1297–1313.

Hammond, P.E., 1958, Geology of the lower Santiago Creek area, San Emigdio Mountains, Kern County, California [M.S. thesis]: University of California, 108 p.

Harding, J.P., Gehrels, G.E., Harwood, D.S., and Girty, G.H., 2000, Detrital zircon geochronology of the Shoo Fly complex, northern Sierra terrane, northeastern California, *in* Soreghan, M.J., and Gehrels, G.E., eds., Paleozoic and Triassic Paleogeography and Tectonics of Western Nevada and Northern California: Geological Society of America Special Paper 347, p. 43–55.

Haxel, G., and Dillon, J., 1978, The Pelona-Orocopia Schist and Vincent-Chocolate Mountain thrust system, southern California, *in* Howell, D.G., and McDougall, K.A., eds., Mesozoic Paleogeography of the Western United States: Pacific Section, Society of Economic Paleontologists and Mineralogists Pacific Coast Paleogeography Symposium 2, p. 453–469.

Henry, D.J., and Dokka, R.K., 1992, Metamorphic evolution of exhumed middle to lower crustal rocks in the Mojave extensional belt, southern California, USA: Journal of Metamorphic Geology, v. 10, p. 347–364, doi:10.1111/j.1525-1314.1992.tb00089.x.

Hofmann, A.W., 2003, Sampling Mantle Heterogeneity through Oceanic Basalts: Isotopes and Trace Elements, *in* Heinrich, D.H., and Karl, K.T., eds., Treatise on Geochemistry 2: Oxford, Pergamon, p. 61–101.

Holland, T., and Blundy, J., 1994, Non-ideal interactions in calcite amphiboles and their bearing on amphibole-plagioclase thermometry: Contributions to Mineralogy and Petrology, v. 116, no. 4, p. 433–447, doi:10.1007/BF00310910.

Hollister, L.S., Grissom, G.C., Peters, E.K., Stowell, H.H., and Sisson, V.B., 1987, Confirmation of the empirical correlation of Al in hornblende with pressure of solidification of calc-alkaline plutons: The American Mineralogist, v. 72, no. 3–4, p. 231–239.

Hopson, R.F., Hillhouse, J.W., and Howard, K.A., 2008, Dike orientations in the Late Jurassic Independence dike swarm and implications for vertical axis tectonic rotations in eastern California: Geological Society of America Special Paper 438, p. 481–498.

House, M.A., Wernicke, B.P., and Farley, K.A., 2001, Paleo-geomorphology of the Sierra Nevada, California, from (U-Th)/He ages in apatite: American Journal of Science, v. 301, no. 2, p. 77–102, doi:10.2475/ajs.301.2.77.

Huffman, O.F., 1972, Lateral displacement of upper Miocene rocks and the Neogene history of offset along the San

Andreas fault in central California: Geological Society of America Bulletin, v. 83, p. 2913–2946, doi:10.1130/0016-7606(1972)83[2913:LDOUMR]2.0.CO;2.

Jacobson, C.E., 1983, Structural geology of the Pelona Schist and Vincent Thrust, San Gabriel Mountains, California: Geological Society of America Bulletin, v. 94, no. 6, p. 753–767, doi:10.1130/0016-7606(1983)94<753:SGOTPS>2.0.CO;2.

Jacobson, C.E., 1995, Qualitative thermobarometry of inverted metamorphism in the Pelona and Rand schists, southern California, using calciferous amphibole in mafic schist: Journal of Metamorphic Geology, v. 13, no. 1, p. 79–92, doi:10.1111/j.1525-1314.1995.tb00206.x.

Jacobson, C.E., Dawson, M.R., and Postlethwaite, C.E., 1988, Structure, metamorphism, and tectonic significance of the Pelona, Orocopia, and Rand schists, southern California, *in* Ernst, W.G., ed., Metamorphism and Crustal Evolution of the Western United States, Rubey Volume 7: New Jersey, Prentice-Hall, p. 976–997.

Jacobson, C.E., Grove, M., Vucic, A., Pedrick, J.N., and Ebert, K.A., 2007, Exhumation of the Orocopia Schist and associated rocks of southeastern California: Relative roles of erosion, synsubduction tectonic denudation, and middle Cenozoic extension: Geological Society of America Special Paper 419, p. 1–37.

Jacobson, C.E., Grove, M., Pedrick, J.N., Barth, A.P., Marsaglia, K.M., Gehrels, G.E., and Nourse, J.A., 2011, Late Cretaceous–early Cenozoic tectonic evolution of the southern California margin inferred from provenance of trench and forearc sediments: Geological Society of America Bulletin, v. 123, no. 3–4, p. 485–506, doi:10.1130/B30238.1.

James, E.W., 1986a, Geochronology, isotopic characteristics, and paleogeography of parts of the Salinian block of California [Ph.D. thesis]: University of California, 176 p.

James, E.W., 1986b, U/Pb age of the Antimony Peak tonalite and its relation to Rand Schist in the San Emigdio Mountains, California: Geological Society of America Abstracts with Programs, v. 18, no. 2, p. 121.

James, E.W., 1992, Cretaceous metamorphism and plutonism in the Santa Cruz Mountains, Salinian block, California, and correlation with the southernmost Sierra Nevada: Geological Society of America Bulletin, v. 104, p. 1326–1339, doi:10.1130/0016-7606(1992)104<1326:CMAPIT>2.3.CO;2.

James, E.W., and Mattinson, J.M., 1985, Evidence for 160 km post-Mid Cretaceous slip on the San Gregorio Fault, coastal California: Eos (Transactions, American Geophysical Union), v. 66, no. 46, p. 1093.

James, E.W., Kimbrough, D.L., and Mattinson, J.M., 1993, Evaluation of displacements of pre-Tertiary rocks on the northern San Andreas fault using U-Pb zircon dating, initial Sr, and common Pb isotopic ratios: Geological Society of America Memoir 178, p. 257–271.

John, D., 1981, Structure and petrology of pelitic schist in the Fremont Peak pendant, northern Gabilan Range, California: Geological Society of America Bulletin, v. 92, no. 5, p. 237–246, doi:10.1130/0016-7606(1981)92<237:SAPOPS>2.0.CO;2.

Johnson, M.C., and Rutherford, M.J., 1989, Experimental calibration of the aluminum-in-hornblende geobarometer with application to Long Valley caldera (California) volcanic rocks: Geology, v. 17, no. 9, p. 837–841, doi:10.1130/0091-7613(1989)017<0837:ECOTAI>2.3.CO;2.

Kanter, L.R., and McWilliams, M.O., 1982, Rotation of the southernmost Sierra Nevada, California: Journal of Geophysical Research, v. 87, B5, p. 3819–3830, doi:10.1029/JB087iB05p03819.

Kidder, S., and Ducea, M.N., 2006, High temperatures and inverted metamorphism in the schist of Sierra de Salinas, California: Earth and Planetary Science Letters, v. 241, no. 3–4, p. 422–437, doi:10.1016/j.epsl.2005.11.037.

Kidder, S., Ducea, M., Gehrels, G.E., Patchett, P.J., and Vervoort, J., 2003, Tectonic and magmatic development of the Salinian Coast Ridge Belt, California: Tectonics, v. 22, doi:10.1029/2002TC001409.

Kistler, R.W., 1990, Two different types of lithosphere in the Sierra Nevada, California, *in* Anderson, J.L., ed., The Nature and Origin of Cordilleran Magmatism: Geological Society of America Memoir 174, p. 271–282.

Kistler, R.W., and Champion, D.E., 2001, Rb-Sr whole-rock and mineral ages, K-Ar, $^{40}Ar/^{39}Ar$, and U-Pb mineral ages, and strontium, lead, neodymium, and oxygen isotopic compositions for granitic rocks from the Salinian Composite Terrane, California: U.S. Geological Survey Open-File Report 01-453, 84 p.

Kistler, R.W., and Peterman, Z., 1973, Variations in Sr, Rb, K, Na and initial $^{87}Sr/^{86}Sr$ in Mesozoic granitic rocks and intruded wall rocks in central California: Geological Society of America Bulletin, v. 84, p. 3489–3512, doi:10.1130/0016-7606(1973)84<3489:VISRKN>2.0.CO;2.

Kistler, R.W., and Peterman, Z.E., 1978, Reconstruction of crustal blocks of California on the basis of initial strontium isotopic compositions of Mesozoic granitic rocks: U.S. Geological Survey Professional Paper 1071, 17 p.

Kistler, R.W., and Ross, D.C., 1990, A strontium isotopic study of plutons and associated rocks of the southern Sierra Nevada and vicinity, California: U. S. Geological Survey Bulletin 1920, 20 p.

Lackey, J.S., Valley, J.W., and Saleeby, J.B., 2005, Supracrustal input to magmas in the deep crust of Sierra Nevada batholith: Evidence from high-$\delta^{18}O$ zircon: Earth and Planetary Science Letters, v. 235, p. 315–330, doi:10.1016/j.epsl.2005.04.003.

Lackey, J.S., Valley, J.W., Chen, J.H., and Stockli, D.F., 2008, Dynamic magma systems, crustal recycling, and alteration in the central Sierra Nevada Batholith: The oxygen isotope record: Journal of Petrology, v. 49, no. 7, p. 1397–1426, doi:10.1093/petrology/egn030.

Lahren, M.L., and Schweickert, R.A., 1989, Proterozoic and Lower Cambrian miogeoclinal rocks of Snow Lake pendant, Yosemite-Emigrant Wilderness, Sierra Nevada, California: Evidence for major Early Cretaceous dextral translation: Geology, v. 17, p. 156–160, doi:10.1130/0091-7613(1989)017<0156:PALCMR>2.3.CO;2.

Leo, G.W., 1967, The plutonic and metamorphic rocks of the Ben Lomond Mountain area, Santa Cruz County, California: California Division of Mines and Geology Special Report, v. 91, p. 27–43.

Li, Y.G., Henyey, T.L., and Silver, L.T., 1992, Aspects of the crustal structure of the western Mojave Desert, California, from seismic reflection and gravity data: Journal of Geophysical Research, v. 97, p. 8805–8816, doi:10.1029/91JB02119.

Liu, L., Spasojevic, S., and Gurnis, M., 2008, Reconstructing Farallon plate subduction beneath North America back to the Late Cretaceous: Science, v. 322, p. 934–938, doi:10.1126/science.1162921.

Liu, L., Gurnis, M., Seton, M., Saleeby, J., Muller, R.D., and Jackson, J., 2010, The role of oceanic plateau subduction in the Laramide orogeny: Nature Geoscience, v. 3, p. 353–357, doi:10.1038/ngeo829.

Ludwig, K.R., 2003, Mathematical-statistical treatment of data and errors for $^{230}Th/U$ geochronology: Reviews in Mineralogy and Geochemistry, v. 52, p. 631–656, doi:10.2113/0520631.

Luffi, P., Saleeby, J.B., Lee, C.A., and Ducea, M.N., 2009, Lithospheric mantle duplex beneath the central Mojave Desert revealed by xenoliths from Dish Hill, California: Journal of Geophysical Research, v. 114, B03202, doi:10.1029/2008JB005906.

Mahéo, G., Saleeby, J., Saleeby, Z., and Farley, K.A., 2009, Tectonic control on southern Sierra Nevada topography, California: Tectonics, v. 28, no. 6, p. TC6006, doi:10.1029/2008TC002340.

Malin, P. E., Goodman, E. D., Henyey, T. L., Li, Y. G., Okaya, D. A., and Saleeby, J. B., 1995, Significance of seismic reflections beneath a tilted exposure of deep continental crust, Tehachapi Mountains, California: Journal of Geophysical Research, v. 100, no. B2, p. 2069–2087, doi: 2010.1029/2094JB02127.

Manuszak, J.D., Satterfield, J.I., and Gehrels, G.E., 2000, Detrital zircon geochronology of Upper Triassic strata in western Nevada: Geological Society of America Special Paper 347, p. 109–118.

Martin, M.W., and Walker, J., 1995, Stratigraphy and paleogeographic significance of metamorphic rocks in the Shadow Mountains, western Mojave Desert, California: Geological Society of America Bulletin, v. 107, no. 3, p. 354–366, doi:10.1130/0016-7606(1995)107<0354:SAPSOM>2.3.CO;2.

Matthews, V., III, 1976, Correlation of Pinnacles and Neenach volcanic fields and their bearing on San Andreas fault problem: The American Association of Petroleum Geologists Bulletin, v. 60, p. 2128–2141.

May, D.J., 1989, Late Cretaceous intra-arc thrusting in southern California: Tectonics, v. 8, no. 6, p. 1159–1173, doi:10.1029/TC008i006p01159.

May, J.C., and Hewitt, R.L., 1948, The basement complex in well samples from Sacramento and San Joaquin Valleys, California: California Division of Mines and Geology Journal, v. 44, p. 129–158.

McWilliams, M.O., and Li, Y., 1983, A paleomagnetic test of the Sierran orocline hypothesis: Eos (Transactions, American Geophysical Union), v. 64, no. 45, p. 686.

Memeti, V., Gehrels, G.E., Paterson, S.R., Thompson, J.M., Mueller, R.M., and Pignotta, G.S., 2010, Evaluating the Mojave–Snow Lake fault hypothesis and origins of central Sierran metasedimentary pendant strata using detrital zircon provenance analyses: Lithosphere, v. 2, no. 5, p. 341–360, doi:10.1130/L58.1.

Miller, E.L., and Sutter, J.F., 1982, Structural geology and ^{40}Ar-^{39}Ar geochronology of the Goldstone–Lane Mountain area, Mojave Desert, California: Geological Society of America Bulletin, v. 93, no. 12, p. 1191–1207, doi:10.1130/0016-7606(1982)93<1191:SGAAGO>2.0.CO;2.

Miller, J.S., Glazner, A.F., Walker, J.D., and Martin, M.W., 1995, Geochronologic and isotopic evidence for Triassic–Jurassic emplacement of the eugeoclinal allochthon in the Mojave Desert region, California: Geological Society of America Bulletin, v. 107, p. 1441–1457, doi:10.1130/0016-7606(1995)107<1441:GAIEFT>2.3.CO;2.

Monastero, F.C., Walker, J.D., Katzenstein, A.M., and Sabin, A.E., 2002, Neogene evolution of the Indian Wells Valley, east-central California: Geological Society of America, v. 195, p. 199–228.

Nadin, E.S., and Saleeby, J.B., 2008, Disruption of regional primary structure of the Sierra Nevada Batholith by the Kern Canyon fault system, California: Geological Society of America Special Paper 438, p. 429–454.

Nelson, C.A., 1962, Lower Precambrian–Cambrian succession, White-Inyo Mountains, California: Geological Society of America Bulletin, v. 73, p. 139–144, doi:10.1130/0016-7606(1962)73[139:LCSWMC]2.0.CO;2.

Nourse, J.A., 1989, Geological evolution of two crustal-scale shear zones: Part I, The Rand thrust complex, northwestern Mojave Desert, California: Part II, The Magdalena metamorphic core complex, north central Sonora, Mexico [Ph.D. thesis]: California Institute of Technology, 394 p.

Nutt, C.J., 1977, The Escondido mafic-ultramafic complex: A concentrically zoned body in the Santa Lucia Range, California [M.S. thesis]: Stanford University, 90 p.

Pearce, J.A., Alabaster, T., Scheton, A.W., and Searle, M.P., 1981, The Oman ophiolite as a Cretaceous arc-basin complex: Evidence and implications: Philosophical Transactions of the Royal Society of London, Series A: Mathematical and Physical Sciences, v. 300, p. 299–317, doi:10.1098/rsta.1981.0066.

Pickett, D.A., and Saleeby, J.B., 1993, Thermobarometric constraints on the depth of exposure and conditions of plutonism and metamorphism at deep levels of the Sierra Nevada Batholith, Tehachapi Mountains, California: Journal of Geophysical Research, v. 98, B1, p. 609–629, doi:10.1029/92JB01889.

Pickett, D.A., and Saleeby, J.B., 1994, Nd, Sr, and Pb isotopic characteristics of Cretaceous intrusive rocks from deep levels of the Sierra Nevada batholith, Tehachapi Mountains, California: Contributions to Mineralogy and Petrology, v.118, no. 2, p. 198–215.

Postlethwaite, C.E., and Jacobson, C.E., 1987, Early history and reactivation of the Rand thrust, southern California: Journal of Structural Geology, v. 9, no. 2, p. 195–205, doi:10.1016/0191-8141(87)90025-3.

Reid, S.A., 1988, Late Cretaceous and Paleogene sedimentation along the east side of the San Joaquin Basin, *in* Graham, S.A., ed., Studies of the Geology of the San Joaquin Basin: Pacific Section, Society of Economic Paleontologists and Mineralogists, v. 60, p. 157–171.

Reiners, P.W., 2005, Zircon (U-Th)/He thermochronometry: Reviews in Mineralogy and Geochemistry, v. 58, no. 1, p. 151–179, doi:10.2138/rmg.2005.58.6.

Reitz, A., 1986, The geology and petrology of the northern San Emigdio plutonic complex, San Emigdio Mountains, southern California [M.A. thesis]: University of California, 80 p.

Rey, P., Vanderhaeghe, O., and Teyssier, C., 2001, Gravitational collapse of the continental crust: Definition, regimes and modes: Tectonophysics, v. 342, p. 435–449, doi:10.1016/S0040-1951(01)00174-3.

Rindosh, M.C., 1977, Geology of the Tylerhorse Canyon pendant southern Tehachapi Mountains Kern County, California [M.S. thesis]: University of Southern California, 80 p.

Ross, D.C., 1970, Quartz gabbro and anorthositic gabbro: Markers of offset along the San Andreas fault in the California Coast Ranges: Geological Society of America Bulletin, v. 81, no. 12, p. 3647–3661, doi:10.1130/0016-7606(1970)81[3647:QGAAGM]2.0.CO;2.

Ross, D.C., 1976, Reconnaissance geologic map of pre-Cenozoic basement rocks, northern Santa Lucia Range, Monterey County, California: U.S. Geological Survey Miscellaneous Field Studies Map MF-750, 7 p.

Ross, D.C., 1977, Pre-intrusive metasedimentary rocks of the Salinian block, California: A paleotectonic dilemma, *in* Stewart, J.H., Stevens, C.H., and Fritsche, A.E., eds., Paleozoic Paleogeography of the Western United States: Pacific Section, Society of Economic Paleontologists and Mineralogists Pacific Coast Paleogeography Symposium 1, p. 371–380.

Ross, D.C., 1988, Chemical traits and trends of the granitic rocks of the southern Sierra Nevada, California: U.S. Geological Survey Open-File Report 88-374, 119 p.

Ross, D.C., 1989, The metamorphic and plutonic rocks of the southernmost Sierra Nevada, California, and their tectonic framework: U.S. Geological Survey Professional Paper 1381, 159 p.

Ross, D.C., Wentworth, C.M., and McKee, E.H., 1973, Cretaceous mafic conglomerate near Gualala offset 350 miles by San Andreas fault from oceanic crustal source near Eagle Rest Peak, California: Journal of Research of the U.S. Geological Survey, v. 1, no. 1, p. 45–52.

Ruppert, S., Fliedner, M.M., and Zandt, G., 1998, Thin crust and active upper mantle beneath the southern Sierra Nevada in the western United States: Tectonophysics, v. 286, p. 237–252, doi:10.1016/S0040-1951(97)00268-0.

Saleeby, J., 1978, Kings River ophiolite, southwest Sierra Nevada foothills, California: Geological Society of America Bulletin, v. 89, no. 4, p. 617–636, doi:10.1130/0016-7606(1978)89<617:KROSSN>2.0.CO;2.

Saleeby, J., 2003, Segmentation of the Laramide slab: Evidence from the southern Sierra Nevada region: Geological Society of America Bulletin, v. 115, no. 6, p. 655–668, doi:10.1130/0016-7606(2003)115<0655:SOTLSF>2.0.CO;2.

Saleeby, J., 2011, Geochemical mapping of the Kings-Kaweah ophiolite belt, California—Evidence for progressive mélange formation in a large offset transform-subduction initiation environment, *in* Wakabayashi, J., and Dilek, Y., eds., Mélanges: Processes of Formation and Societal Significance: Boulder, Colorado, Geological Society of America Special Paper 480, p. 31–73, doi:10.1130/2011.2480(02)

Saleeby, J.B., and Busby, C., 1993, Paleogeographic and tectonic setting of axial and western metamorphic framework rocks of the southern Sierra Nevada, California: Field Trip Guidebook, Pacific Section, Society of Economic Paleontologists and Mineralogists, v. 71, p. 197–225.

Saleeby, J., and Sharp, W., 1980, Chronology of the structural and petrologic development of the southwest Sierra Nevada foothills, California: Geological Society of America Bulletin, v. 91, no. 6, p. 317–320, doi:10.1130/0016-7606(1980)91<317:COTSAP>2.0.CO;2.

Saleeby, J.B., Sams, D.B., and Kistler, R.W., 1987, U/Pb zircon, strontium, and oxygen isotopic and geochronological study of the southernmost Sierra Nevada Batholith, California: Journal of Geophysical Research, v. 92, B10, p. 10,443–10,466, doi:10.1029/JB092iB10p10443.

Saleeby, J.B., Ducea, M.N., and Clemens-Knott, D., 2003, Production and loss of high-density batholithic root, southern Sierra Nevada, California: Tectonics, v. 22, doi:10.1029/2002TC001374.

Saleeby, J., Farley, K.A., Kistler, R.W., and Fleck, R.J., 2007, Thermal evolution and exhumation of deep-level batholithic exposures, southernmost Sierra Nevada, California: Geological Society of America Special Paper 419, p. 39–66.

Saleeby, J.B., Ducea, M.N., Busby, C.J., Nadin, E.S., and Wetmore, P.H., 2008, Chronology of pluton emplacement and regional deformation in the southern Sierra Nevada Batholith, California: Geological Society of America Special Paper 438, p. 397–427.

Saleeby, J.B., Saleeby, Z., Chapman, A.D., and Nadin, E.S., 2009a, Origin and evolution of the White Wolf Fault and the Maricopa Basin (MB), southernmost Great Valley (GV), California: Geological Society of America Abstracts with Programs, v. 41, no. 7, p. 180.

Saleeby, J.B., Saleeby, Z., Nadin, E., and Mahéo, G., 2009b, Step-over in the structure controlling the regional west tilt of the Sierra Nevada microplate: Eastern escarpment system to Kern Canyon system: International Geology Review, v. 51, no. 7–8, p. 634–669, doi:10.1080/00206810902867773.

Schmidt, M.W., 1992, Amphibole composition in tonalite as a function of pressure: An experimental calibration of the Al-in-hornblende barometer: Contributions to Mineralogy and Petrology, v. 110, no. 2–3, p. 304–310, doi:10.1007/BF00310745.

Schott, R.C., and Johnson, C.M., 1998, Sedimentary record of the Late Cretaceous thrusting and collapse of the Salinia-Mojave magmatic arc: Geology, v. 26, no. 4, p. 327–330, doi:10.1130/0091-7613(1998)026<0327:SROTLC>2.3.CO;2.

Schott, R.C., and Johnson, C.M., 2001, Garnet-bearing trondhjemite and other conglomerate clasts from the Gualala Basin, California: Sedimentary record of the missing western portion of the Salinian magmatic arc?: Geological Society of America Bulletin, v. 113, no. 7, p. 870–880, doi:10.1130/0016-7606(2001)113<0870:GBTAOC>2.0.CO;2.

Simpson, C., 1990, Microstructural evidence for northeastward movement on the Chocolate Mountains fault zone, southeastern California: Journal of Geophysical Research, v. 95, B1, p. 529–537, doi:10.1029/JB095iB01p00529.

Smith, M., and Gehrels, G., 1994, Detrital zircon geochronology and the provenance of the Harmony and Valmy Formations, Roberts Mountains allochthon, Nevada: Geological Society of America Bulletin, v. 106, no. 7, p. 968–979, doi:10.1130/0016-7606(1994)106<0968:DZGATP>2.3.CO;2.

Snoke, A.W., Sharp, W.D., Wright, J.E., and Saleeby, J.B., 1982, Significance of mid-Mesozoic peridotitic to dioritic intrusive complexes, Klamath Mountains–western Sierra Nevada, California: Geology, v. 10, no. 3, p. 160–166, doi:10.1130/0091-7613(1982)10<160:SOMPTD>2.0.CO;2.

Spear, F.S., 1993, Metamorphic phase equilibria and pressure-temperature-time paths: Washington, D.C., Mineralogical Society of America, 799 p.

Stevens, C.H., and Greene, D.C., 1999, Stratigraphy, depositional history, and tectonic evolution of Paleozoic continental-margin rocks in roof pendants of the eastern Sierra Nevada, California: Geological Society of America Bulletin, v. 111, no. 6, p. 919–933, doi:10.1130/0016-7606(1999)111<0919:SDHATE>2.3.CO;2.

Stevens, C.H., and Stone, P., 2005, Interpretation of the Last Chance Thrust, Death Valley region, California, as an Early Permian décollement in a previously undeformed shale basin: Earth-Science Reviews, v. 73, no. 1–4, p. 79–101, doi:10.1016/j.earscirev.2005.04.005.

Sun, S., and McDonough, W.F., 1989, Chemical and isotopic systematics of oceanic basalts: Implications for mantle composition and processes, *in* Saunders., A.D., and Norry, M.J., eds., Magmatism in the Ocean Basins: The Geological Society of London Special Publication 42, p. 313–345.

Trask, P.D., 1926, Geology of Point Sur Quadrangle, California: University of California Publications in Geological Sciences, v. 16, no. 6, p. 119–186.

Walker, J.D., 1988, Permian and Triassic rocks of the Mojave Desert and their implications for timing and mechanisms of continental truncation: Tectonics, v. 7, no. 3, p. 685–709, doi:10.1029/TC007i003p00685.

Wiebe, R.A., 1966, Structure and petrology of Ventana Cones area, California [Ph.D. thesis]: Stanford University, 95 p.

Wiebe, R.A., 1970, Pre-Cenozoic tectonic history of the Salinian Block, western California: Geological Society of America Bulletin, v. 81, p. 1837–1842, doi:10.1130/0016-7606(1970)81[1837:PTHOTS]2.0.CO;2.

Williams, H., and Curtis, G.H., 1976, The Sutter Buttes, a study of Plio-Pleistocene volcanism: University of California Publications in Geological Sciences: University of California Press, v. 116, p. 1–56.

Wolf, M.B., and Saleeby, J.B., 1995, Late Jurassic dike swarms in the southwestern Sierra Nevada Foothills Terrane, California: Implications for the Nevadan orogeny and North American plate motion: Geological Society of America Special Paper 299, p. 203–228.

Wood, D.J., 1997, Geology of the eastern Tehachapi Mountains and Late Cretaceous–early Cenozoic tectonics of the southern Sierra Nevada region, Kern County, California [Ph.D. thesis]: California Institute of Technology, 287 p.

Wood, D.J., and Saleeby, J.B., 1997, Late Cretaceous–Paleocene extensional collapse and disaggregation of the southernmost Sierra Nevada Batholith: International Geology Review, v. 39, no. 11, p. 973–1009, doi:10.1080/00206819709465314.

Yan, Z., Clayton, R.W., and Saleeby, J., 2005, Seismic refraction evidence for steep faults cutting highly attenuated continental basement in the central Transverse Ranges, California: Geophysical Journal International, v. 160, p. 651–666, doi:10.1111/j.1365-246X.2005.02506.x.

Manuscript Received 20 July 2011
Revised Manuscript Received 23 November 2011
Manuscript Accepted 25 November 2011